Chapter 14: Deformation of Single Layers

SINGLE ROCK-LAYERS of compositions different from their host rock (veins, dikes, primary beds) may deform into ptygmatic folds, boudins, mullions, dome-and-basin folds, and chocolate-tablet boudinage. The change in length and orientation of lines, during progressive deformation, can be used to understand when single layer structures form and what their orientation is with respect to the principal directions of strain.

The approximate orientation of folds and boudins with respect to the shortening direction in pure shear is outlined in section 14-1. Expressions for the general stretch of arbitrary lines in any strain ellipse are given in section 14-2. The incremental and finite strain ellipses for pure and simple shear are introduced in sections 14-3 to 14-6. The strain history ellipse and the meaning of its internal segments are explained in section 14-7. Dome-and-basin folds and chocolate-tablet boudinage, structures formed by the deformation of competent single layers, are outlined in section 14-8. Equations for the rotation of material lines and planes in coaxial 3D deformations are given in section 14-9. Subsequently, the surface-of-no-finite-strain is discussed in section 14-10. Progressive deformation of competent single layers in 3D is outlined in section 14-11.

Practical hint: **The formation of boudins, folds, and mullions has been simulated in analog experiments, using viscous model materials. But the detailed shape of so-called inverse folds is still poorly constrained (see Figure 14-20 and text on page 248). Attempt to run a laboratory experiment to visualize and study the development of inverse folds in analog models.**

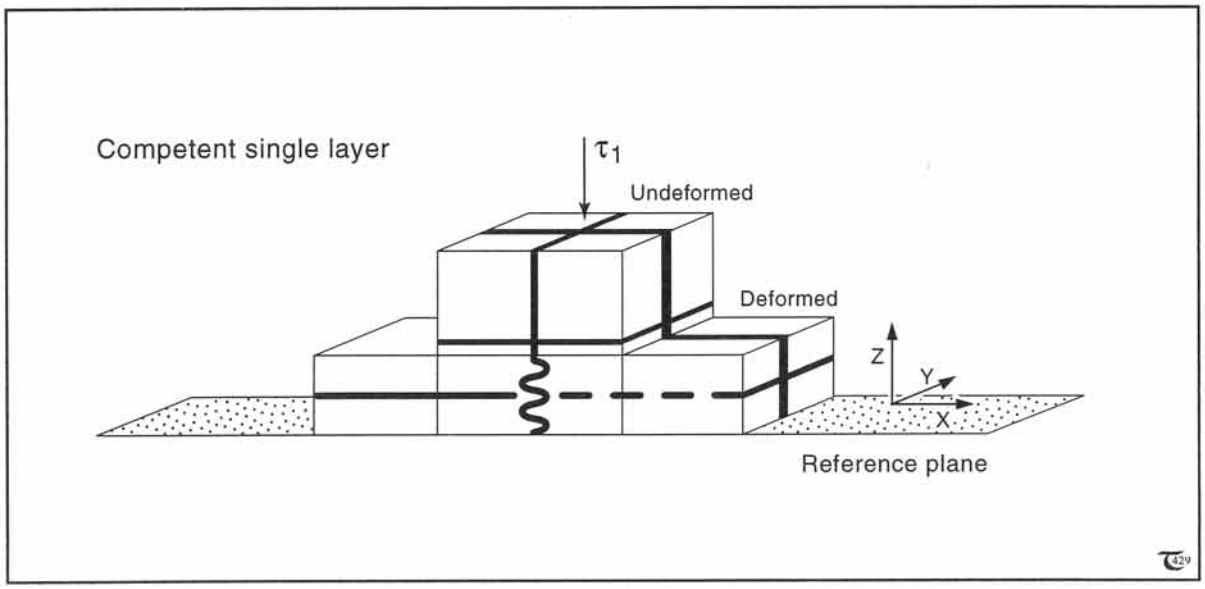

Figure 14-1: *The orientation of buckling and boudinaging of competent single layers with respect to the directions of shortening and extension.*

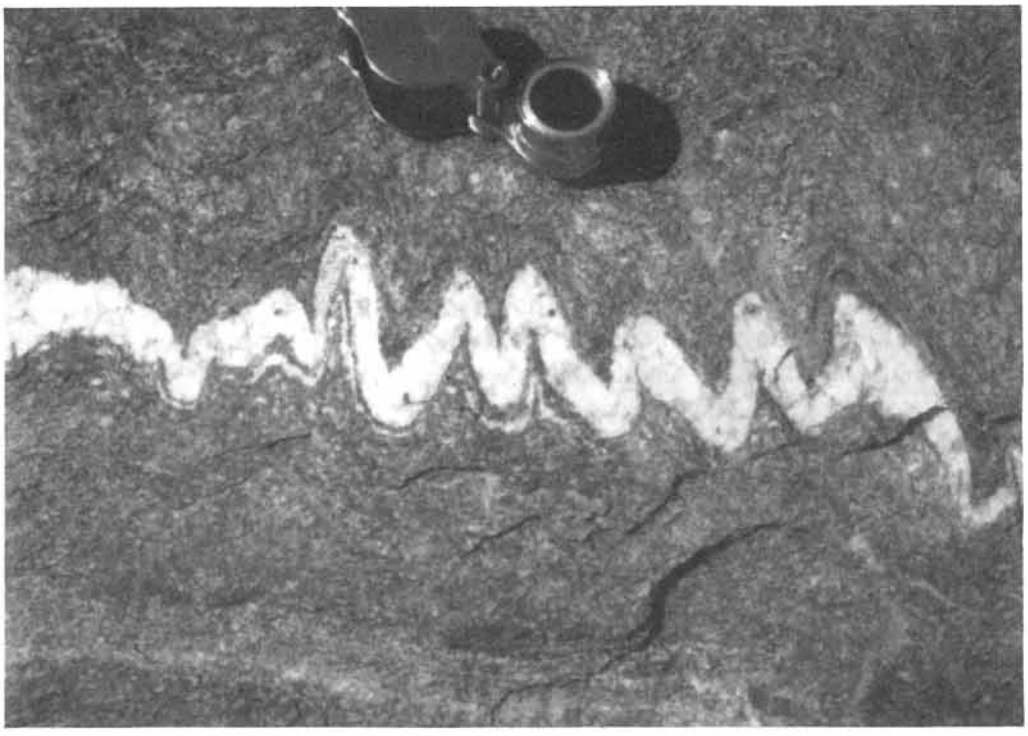

Figure 14-2a: *Ptygmatic folds in competent single layer of quartz, embedded within granite gneiss of Khamis Mushayt, Saudi Arabia.*

14-1 Instabilities of single layers

Single layers will either fold or boudinage - depending on their orientation with respect to the shortening directions - if deforming together with mechanically weaker country rock (Fig. 14-1). Such single layers are more *competent* than the surrounding, *incompetent* rock. Attempts to shorten competent single layers cause symmetric (and sometimes asymmetric) folding (Fig. 14-2a). The ptygmatic folding of competent single layers has been confirmed by extensive numerical and analog modeling in tectonic laboratories. It has, also, been demonstrated that extension of competent layers causes them to develop necks or pinch-and-swell structures, which can separate into boudins (Fig. 14-2b). All these deformation structures result from the resistance of competent single layers to changes in their length at the distortion rate dictated by the large volume of relatively incompetent host rock.

Figure 14-2b: *Pre-boudinage, pinch-and-swell stage of deformation, in competent single aplite vein within greenschist host rock, Khamis Mushayt, Saudi Arabia.*

Figures 14-3a to c illustrate a progressive deformation with the position of four material lines marked. Shown are the initial, undeformed state and two subsequent stages of deformation. The passive material lines, labelled A to D, have to change their lengths during the deformation. They, also, rotate away from the shortening direction. Figures 14-4a to d plot the change in the stretches for each of the four lines, used in Figure 14-3. The length history of these lines

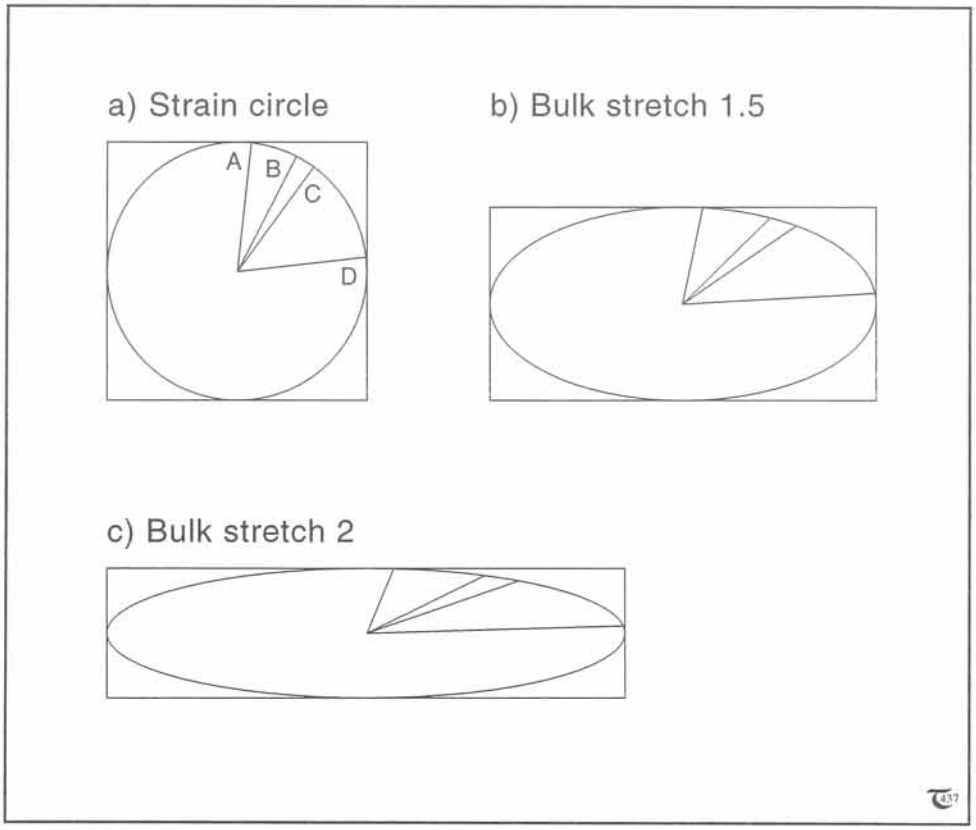

Figure 14-3: *a) to c) Rotation and stretch of material lines, A to D, in progressive deformation by pure shear.*

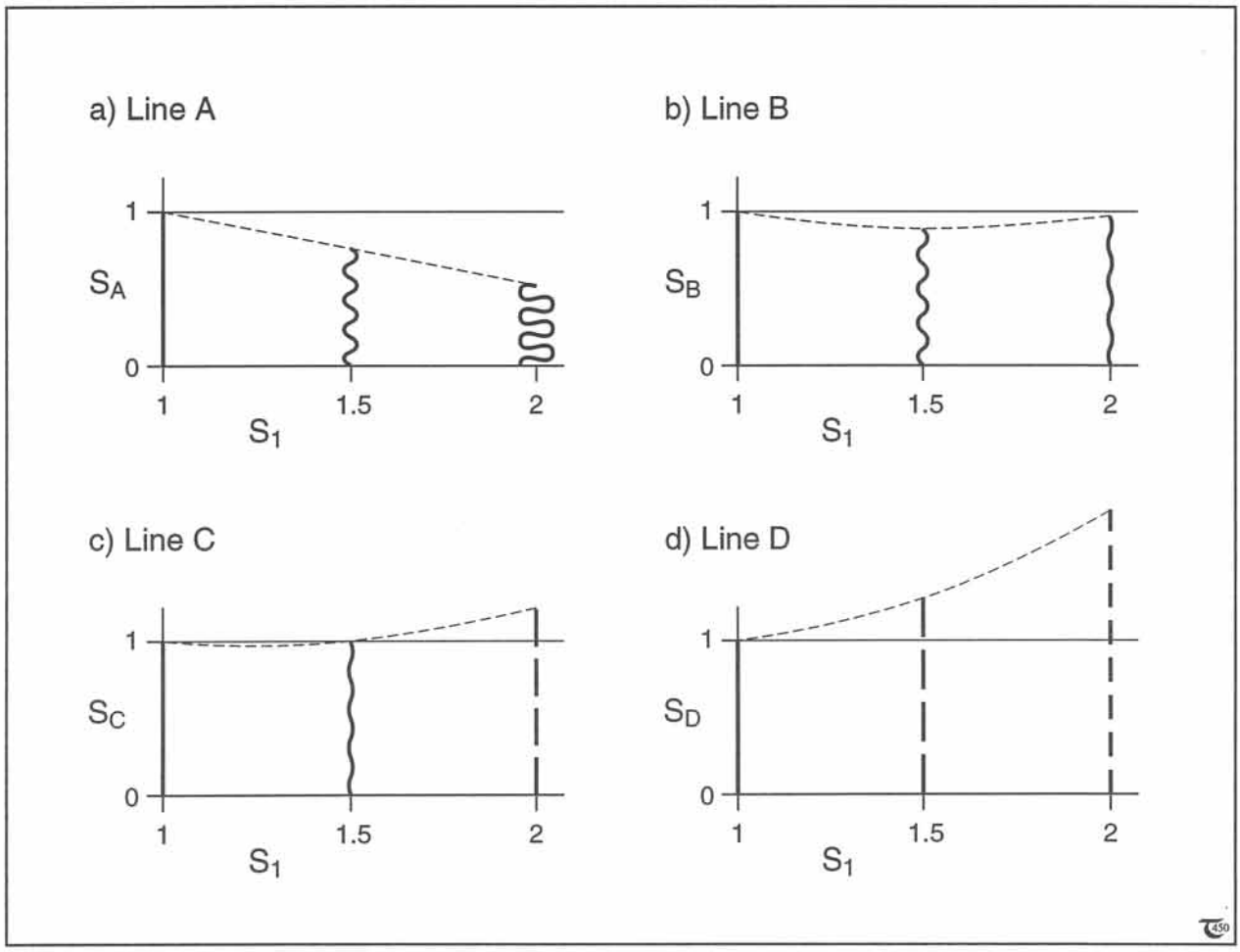

Figure 14-4: *a) to d) Stretch history of material lines, A to D, illustrated in the deformation stages of Figures 14-3 a to c.*

shows that lines which are initially close to the shortening direction (A, B, and C) first shorten and then extend.

14-2 Length of lines in 2D strain

The length history of an arbitrary line, valid for any general 2D strain development, is given here. The stretch, S_ϕ, of an arbitrary material line oriented at angle ϕ away from the major principal stretch axis, S_1, can be calculated from the magnitude of the two principal stretches (Figs. 14-6a & b):

$$S_\phi = (S_1^2\cos^2\phi + S_3^2\sin^2\phi)^{1/2} = [S_1^2\cos^2\phi + (1/S_1)^2\sin^2\phi]^{1/2} \qquad (14\text{-}1)$$

Figure 14-6c graphs S_ϕ against ϕ, using equation (14-1) with S_1-values of 1, 2, 3, 4, and 5. The *initial* orientation, α_0 (or ϕ_0), of the material line considered (Fig. 14-6a) cannot be determined retrospectively. It depends upon the mode of deformation and is different, for example, for pure and simple shear.

Although some material lines are extending and others are shortening, or both, all lines will be longer than the shortest principal stretch, S_3, at any time. The *proportional stretch*, i.e. the stretch, S_ϕ, normalized by the smallest principal stretch, S_3, is:

$$S_\phi/S_3 = [R^2/(\cos^2\phi + R^2\sin^2\phi)]^{1/2} \qquad (14\text{-}2a)$$

☐Exercise 14-1: Figure 14-5 is a field picture of a folded multilayer. The dark rocks are calc-silicates, and the white rocks are marbles. Carefully study the structure of the deformed multilayer, and answer the following questions. a) Which rock is more competent, the marble or the calc-silicate? b) Mark the directions of shortening and extension on the outcrop. c) Explain why both folds and boudinage occur in this deformation pattern.

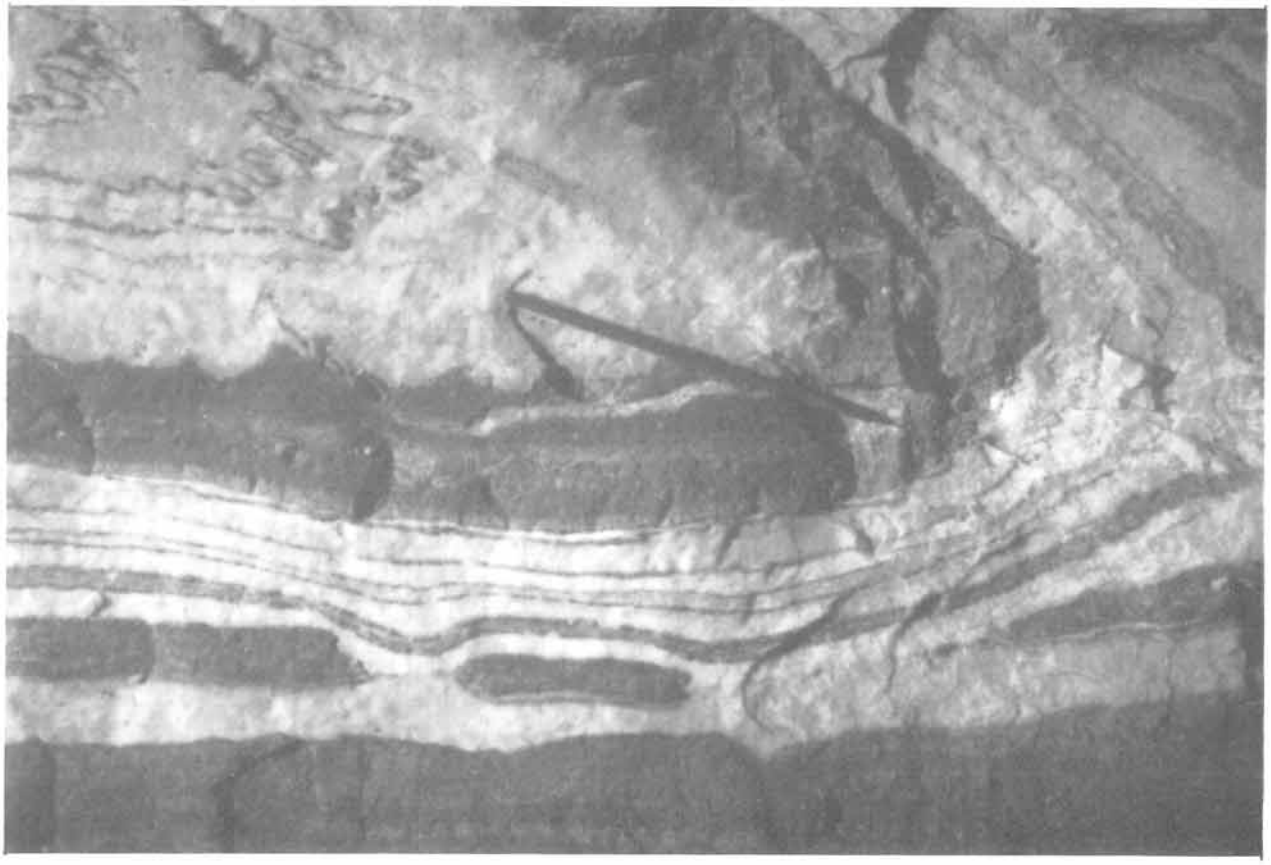

Figure 14-5: *Concentric fold and boudinaged limbs of calc-silicate beds (dark) in marble (white) host rock. Khan Gorge, Namibia. Courtesy John Ramsay.*

with ellipticity $R=S_1/S_3=S_1^2$ for plane strain, so that:

$$S_\phi/S_3=[S_1^4/(\cos^2\phi+S_1^4\sin^2\phi)]^{1/2} \qquad (14\text{-}2b)$$

The function of equation (14-2b) is plotted in Figure 14-7, which emphasizes that the stretch, S_ϕ, of a line close to the maximum extension, S_1 (for $\phi=0$), increases much faster with progressive strain than those still further away from S_1. Eventually all material lines will rotate towards the major stretch direction, S_1, and the proportional stretch of any material line approaches S_1/S_3 after sufficiently large finite straining.

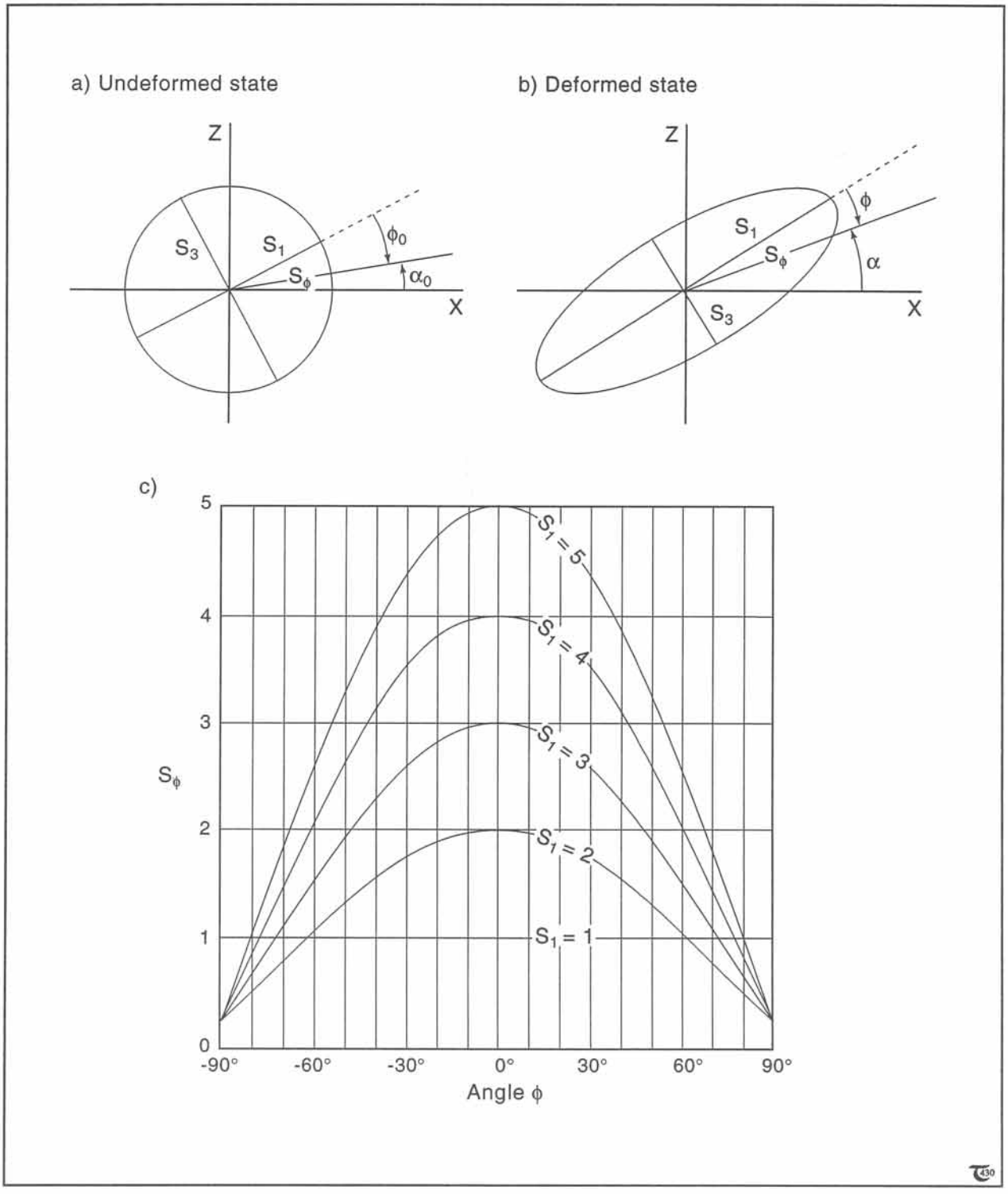

Figure 14-6a to c: *(a & b) Deformation sketches for material line with stretch, S_ϕ, oriented at angle ϕ away from the major stretching axis. (c) Stretching history graph of S_ϕ for a range of final orientations, ϕ, and finite strains, S_1, using equation (14-1).*

☐Exercise 14-2: Study the deformation patterns of Figures 14-8a and b, overleaf. Discuss for each of the deformed layers a possible stretching history, that could explain their present appearance.

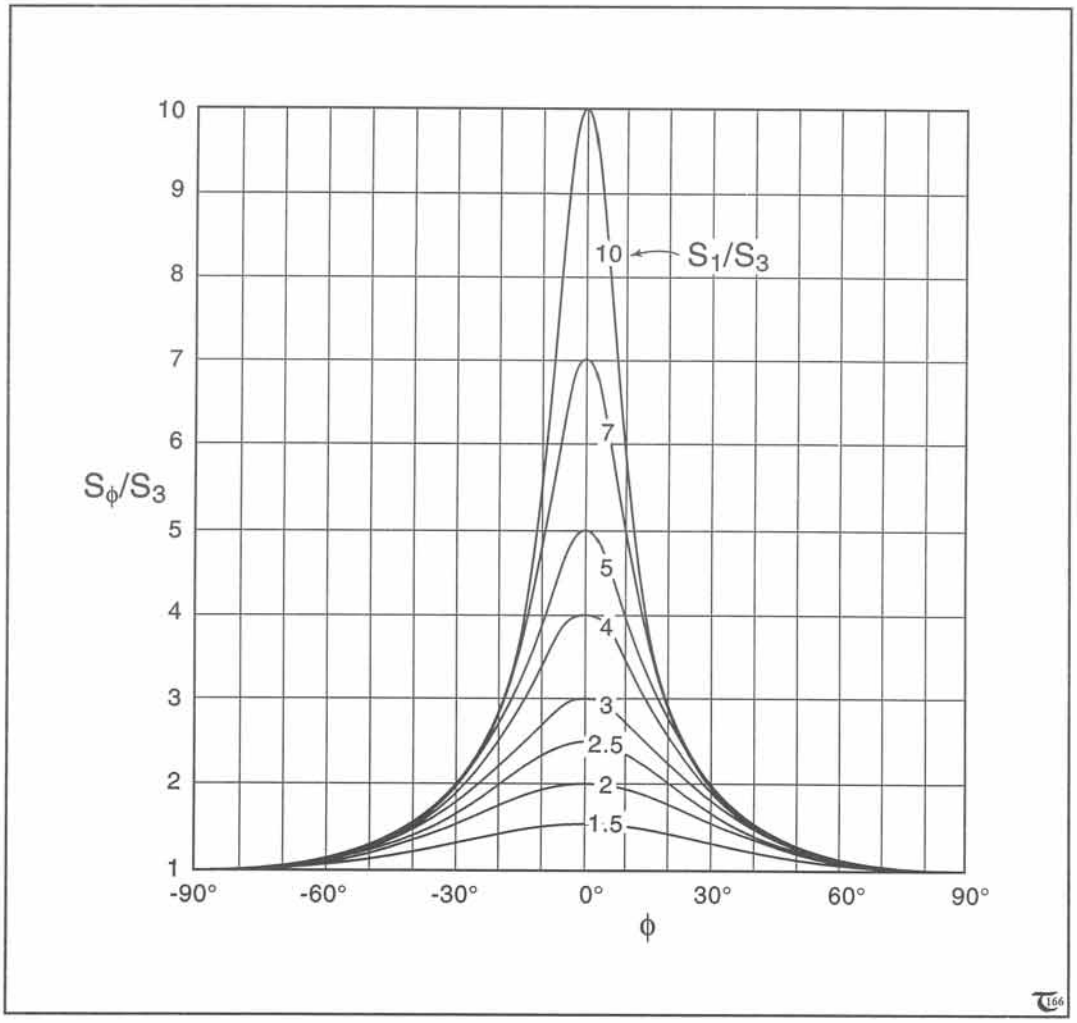

Figure 14-7: *Graph similar to that of Figure 14-6c, but both S_ϕ and S_1 are re-normalized by S_3, using equation (14-2b).*

Figure 14-8a: *Ptygmatic folds in competent pegmatite vein in meta-sedimentary rocks of Moine, Mull, Scotland. Courtesy John Ramsay.*

Figure 14-8b: *Folded boudins in amphibolite gneiss sequence, Lower Penninic nappes, Ticino, Switzerland. Courtesy John Ramsay.*

14-3 Incremental strain ellipse for pure shear

In order to understand still better the deformation history, experienced by material lines and planes in rock of homogeneous *bulk deformation*, it is useful to consider the deformation as the result of small increments of distortion. The small amount of strain, accumulated during the first increment of time in a progressive distortion, can be represented by an *incremental strain ellipse*. This ellipse is only slightly departing from the undistorted strain circle. Geoscience sometimes uses the term *infinitesimal strain ellipse* for incremental or small strains. This use of infinitesimal strains should not be confounded with the alternative use in *infinitesimal deformation*, which sometimes refers to the deformation in *small volumes*, which still may involve large finite strains, rather than small strains.

The incremental strain ellipse of pure shear deformation can be superimposed onto the initial, undistorted strain circle to compare their shapes. Their superimposition divides any rock volume into sections, where material lines are either slightly shortened or extended (Fig. 14-9). The sectors of shortening and extension are separated by the two imaginary lines, A, that have neither extended nor shortened and, therefore, are termed *lines-of-no-infinitesimal-strain*. The two imaginary lines-of-no-infinitesimal-strain are always mutually perpendicular, and their orientation is stationary at 45° to the instantaneous shortening direction. Any material lines that initially coincide with these lines, A, will rotate into the field of extension if another increment of strain is added. (These rotated material lines are marked A^* in Figure 14-15; see section 14-5).

The *rotation of an arbitrary material line*, initially at angle α_0 and changed into α after the stretch, can be determined from (Figs. 14-10a & b):

$$\tan \alpha = (S_3/S_1)\tan \alpha_0 = S_1^{-2} \tan \alpha_0 \qquad (14\text{-}3a)$$

This relationship is valid only for pure shear deformations, unlike equation (14-1) and the situation in Figures 14-6a & b, which is valid for any plane strain. Figure 14-10c graphs the orientation, α, of the line rotated after deformation against S_1 for a range of initial values for α_0, using equation (14-3a). The coeval *change in the normalized length* of the line, S_α, during the rotation is (Figs. 14-10a & b):

$$S_\alpha = S_1 \cos \alpha_0 / \cos \alpha = S_1 \cos \alpha_0 / \cos[\tan^{-1}(S_1^{-2} \tan \alpha_0)] \qquad (14\text{-}3b)$$

Figure 14-10d plots S_α versus S_1, using equation (14-3b) for a range of α-values.

The future orientation, α_{A^*}, of material lines, A^*, that were initially the 45° lines-of-no-infinitesimal-strain, A, can be calculated from equation

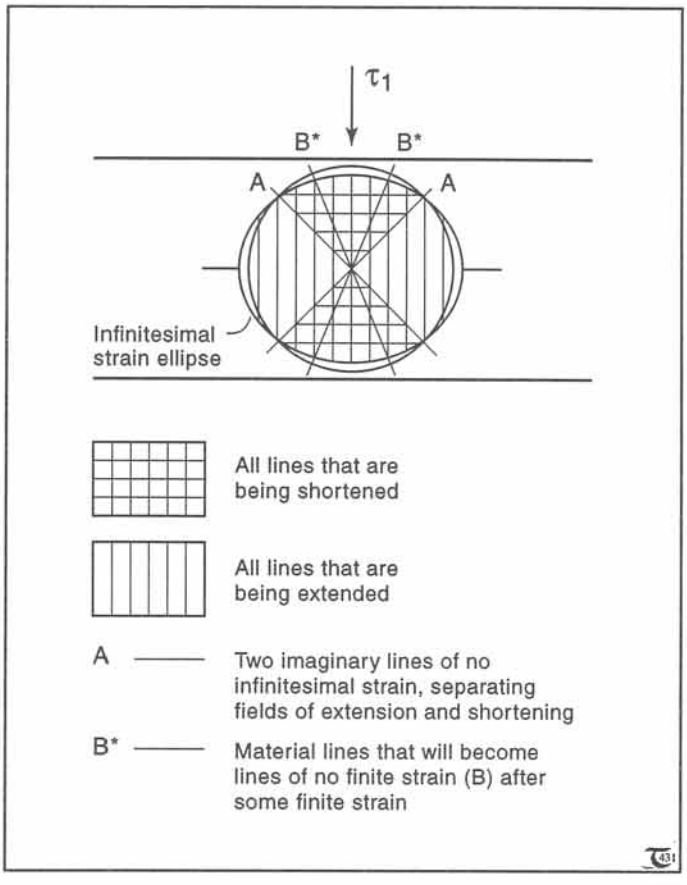

Figure 14-9: *Infinitesimal or incremental strain ellipse for pure shear deformation. See, also, Figure 14-15.*

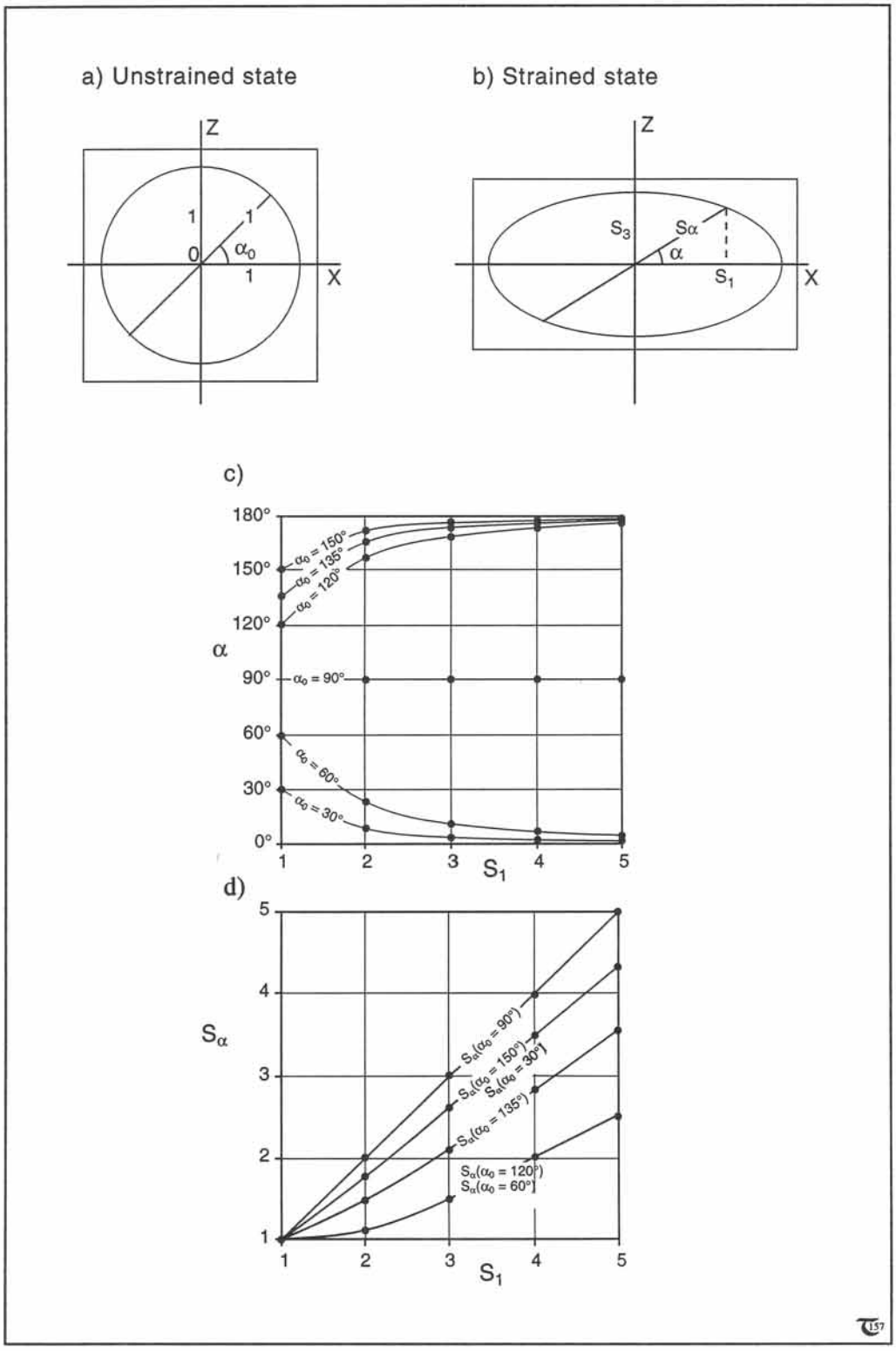
a) Unstrained state
b) Strained state
Z
X
1
1
0
α_0
1
S_3
$S\alpha$
α
S_1
c)
180°
150°
120°
90°
60°
30°
0°
α
$\alpha_0 = 150°$
$\alpha_0 = 135°$
$\alpha_0 = 120°$
$\alpha_0 = 90°$
$\alpha_0 = 60°$
$\alpha_0 = 30°$
1 2 3 4 5
S_1
d)
5
4
3
2
1
S_α
$S_\alpha(\alpha_0 = 90°)$
$S_\alpha(\alpha_0 = 150°)$
$S_\alpha(\alpha_0 = 30°)$
$S_\alpha(\alpha_0 = 135°)$
$S_\alpha(\alpha_0 = 120°)$
$S_\alpha(\alpha_0 = 60°)$
1 2 3 4 5
S_1

Figure 14-10a to d: *(a & b) Material lines with stretch, S_α, oriented at angle α away from the major stretching axis, S_1; before and after deformation.*
(c & d) Change in orientation, α, and stretch, S_α, for lines with a range of initial orientations, α_0, versus increasing major principal stretch, S_1. See equation (14-3a & b).

(14-3a), taking $\alpha_0=45°$ and using $S_1=1/S_3$ (for isochoric plane strain):

$$\alpha_{A*}=\tan^{-1}(S_3/S_1)=\tan^{-1}(S_1^{-2}) \qquad (14\text{-}4)$$

Figure 14-11 graphs the rotation history of the angles, α_{A*}, against S_1 for pure shear. Remember that $\alpha_{A*}=45°$ for $S_1=1$ at the onset of the deformation.

☐Exercise 14-3: Examine Figure 14-9. Color the ellipse sectors of instantaneous shortening and extension differently.
a) What is the orientation of lines A? b) Explain why lines A and the *material lines* at 45° to the shortening direction are, in fact, very different.

Figure 14-11: *Rotation of the material lines, A^*, that were initially at 45° to the shortening direction. These initial lines, of no infinitesimal strain at the onset of pure shear deformation, rotate over α_{A*}, as S_1 increases. See equation (14-4).*

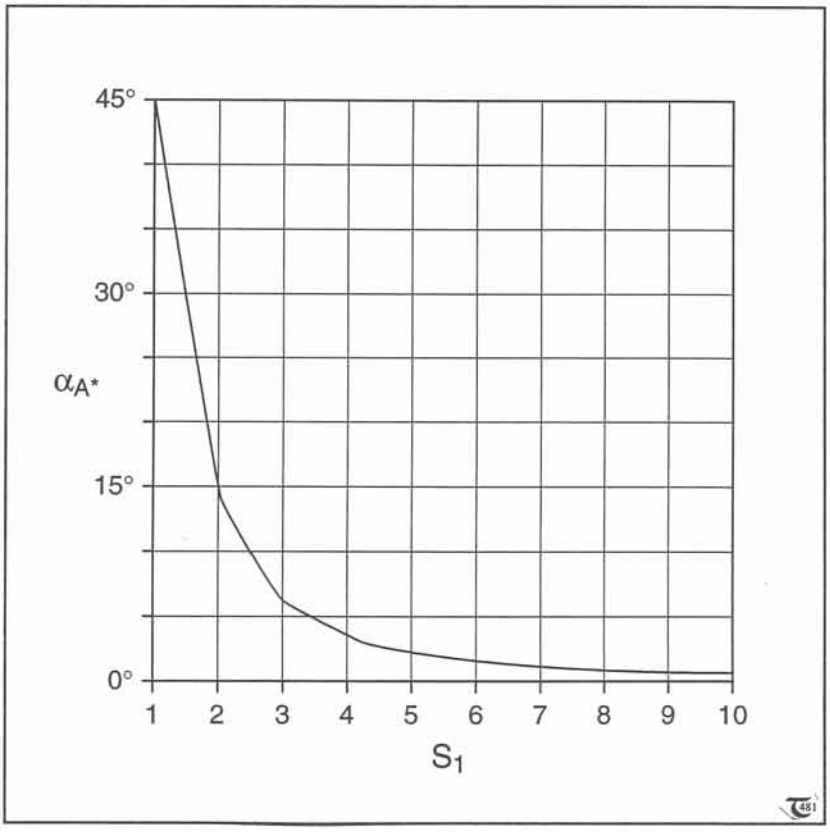

☐Exercise 14-4: Material lines within the cubic rock volume of Figure 14-10a all rotate away from the Z-axis. a) What is the ultimate orientation of the material lines after very large strain? b) Which material lines do not rotate at all? c) Which material lines rotate fastest?

☐Exercise 14-5: Examine the graph of Figure 14-10d. Which material line is stretching fastest?

☐Exercise 14-6: Figure 14-10d does not include the stretch history of material lines with initial orientations $\alpha_0=70°$, 80°, and 89°. a) Plot S_α for these lines in Figure 14-10d, extending the vertical scale downward if necessary. b) Explain the result.

14-4 Incremental strain ellipse for simple shear

Figure 14-12 shows a simple shear deformation. The orientation of the principal incremental strain axes, in simple shear, can be found at 45° to the direction of shear. The principal axes of incremental strain fix the orientation of the lines-of-no-infinitesimal-strain at 45° with respect to the major shortening direction. Consequently, lines-of-no-infinitesimal-strain are always parallel and normal to the direction of shear. Again, any material lnes that initially coincide with these lines, A, will rotate into the field of extension if another increment of strain is added. (These rotated material lines are marked A^* in Figure 14-17; see section 14-6).

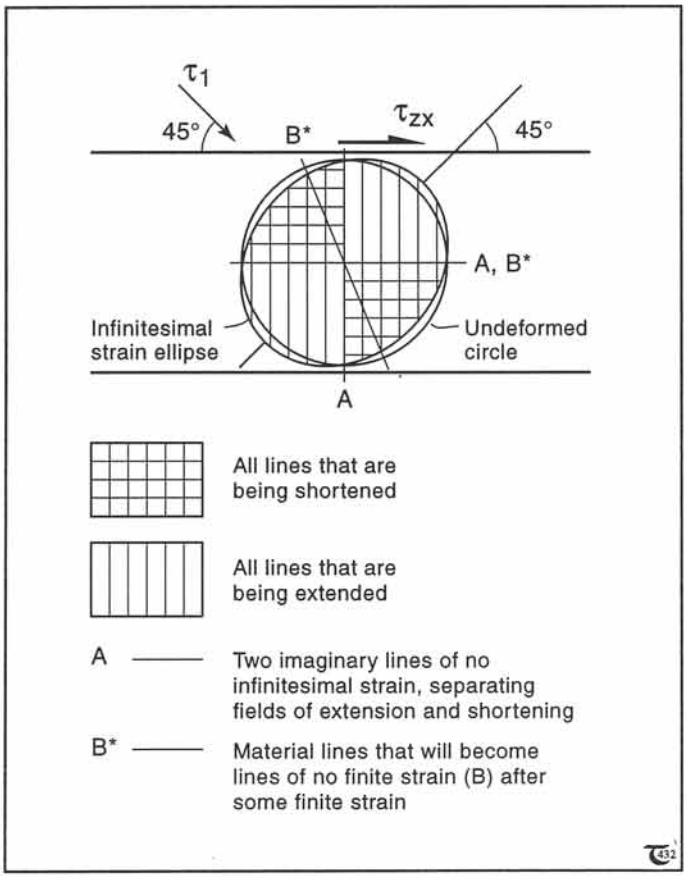

Figure 14-12: *Infinitesimal or incremental strain ellipse for simple shear deformation. See, also, Figure 14-17.*

The *rotation of an arbitrary material line*, initially at angle α_0 will change into α after the stretch and can be determined from (Figs. 14-13a & b):

$$\cot \alpha = \gamma + \cot \alpha_0 \qquad (14\text{-}5a)$$

Figure 14-13c graphs the orientation of the rotated line, α, against the angular shear strain, γ, for a range of initial values of α_0, using equation (14-5a). The coeval *change in the normalized length* of the line, S_α, during the rotation is (Figs. 14-13a & b):

$$S_\alpha = (1 - 2\gamma \cos \alpha_0 \sin \alpha_0 + \gamma^2 \sin^2 \alpha_0)^{1/2} \qquad (14\text{-}5b)$$

Figure 14-13d plots S_α versus γ using equation (14-5b) for a range of values, α_0.

The future orientation, α_{A*}, of material lines, A^*, that were initially the lines-of-no-infinitesimal-strain, A (Fig. 14-12), can be calculated from equation (14-5a), taking $\alpha_0 = 45°$:

$$\alpha_{A*} = \cot^{-1}\gamma = \tan^{-1}\gamma^{-1} \qquad (14\text{-}6)$$

This expression, valid for simple shear deformation only, is graphed with α_{A*} versus γ in Figure 14-14. Recall that $\alpha_{A*} = 90°$ for $\gamma = 0$.

☐Exercise 14-7: Examine Figure 14-12. Color the ellipse sectors of instantaneous shortening and extension. a) What is the orientation of lines A? b) Why do lines A and B^*, both parallel to the direction of shear, coincide?

☐Exercise 14-8: Examine Figure 14-13c, and conclude for which orientation, α_0, material lines do not rotate at all, in simple shear.

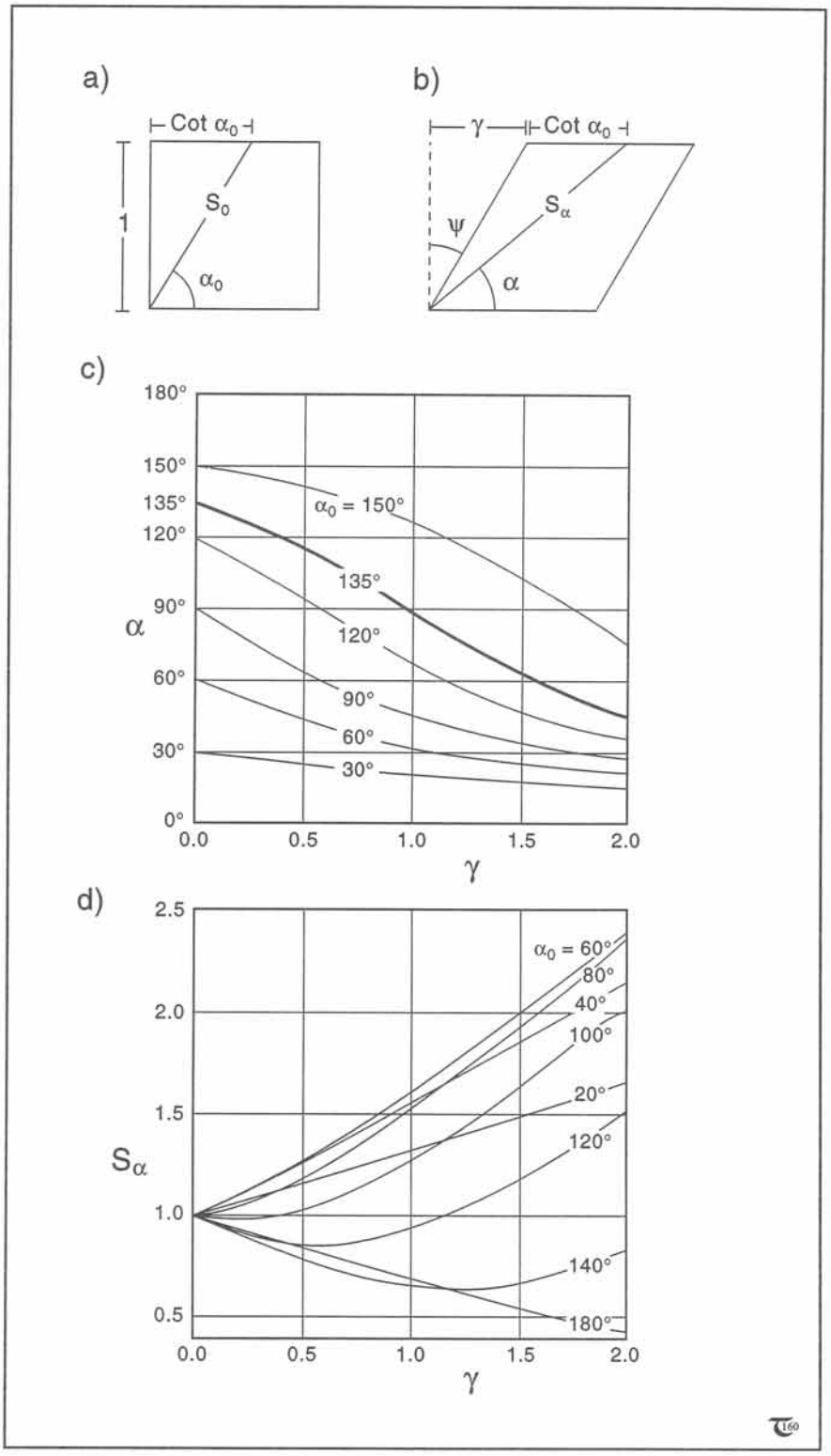

Figures 14-13a to d: *(a & b) Material lines with stretch, S_α, oriented at α, away from the direction of shear; shown before at (a) and after deformation at (b).*
(c & d) Change in orientation, α, and stretch, S_α, for lines with a range of initial orientations, α_0, versus increasing angular shear strain, γ. See equations (14-5a & b).

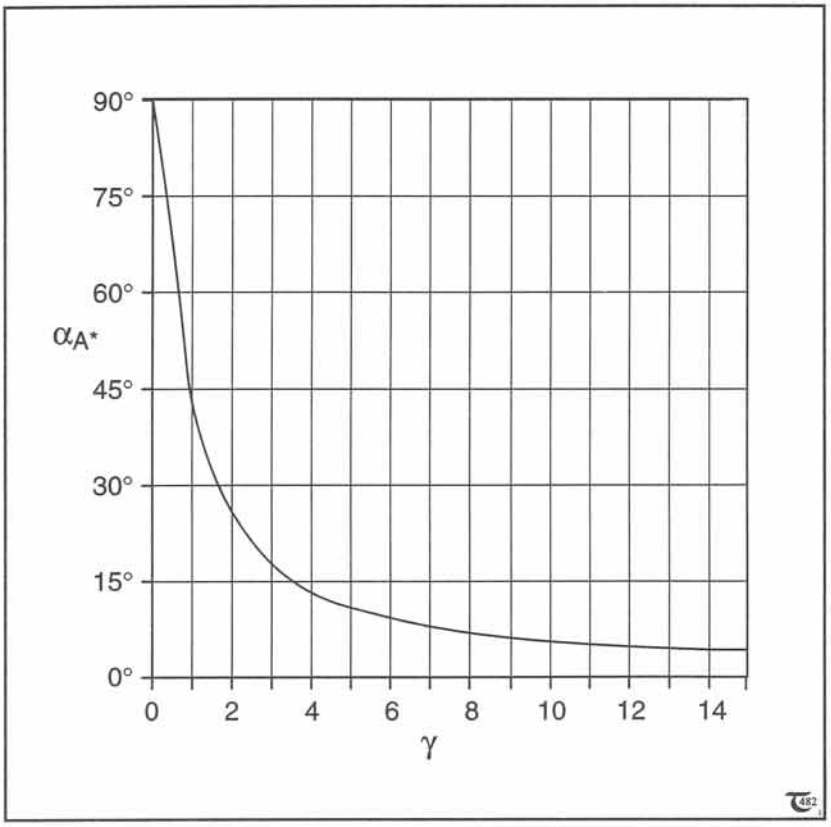

Figure 14-14: *Rotation of the material lines, A^*, that were initially parallel and normal to the shear direction. These initial lines, of no infinitesimal strain at the onset of simple shear deformation, rotate over α_{A^*}, as γ increases. See equation (14-6).*

□Exercise 14-10: The angle $(\alpha_{B^*}-\alpha_B)$, indicated in Figure 14-16 measures the total rotation, experienced by material lines that become lines-of-no-finite-strain, B^*. a) Produce a separate graph of $(\alpha_{B^*}-\alpha_B)$ versus S_1. b) Explain the implication of this plot for the volume of rock still not shortened after a principal stretch of 6.

□Exercise 14-9: Examine Figure 14-15. Color the ellipse sectors of finite shortening and extension, using colors different from those used in exercise 14-3a. Establish the finite strain in Figure 14-15, and check whether the lines A^* are in the appropriate orientation, using the graph of Figure 14-11.

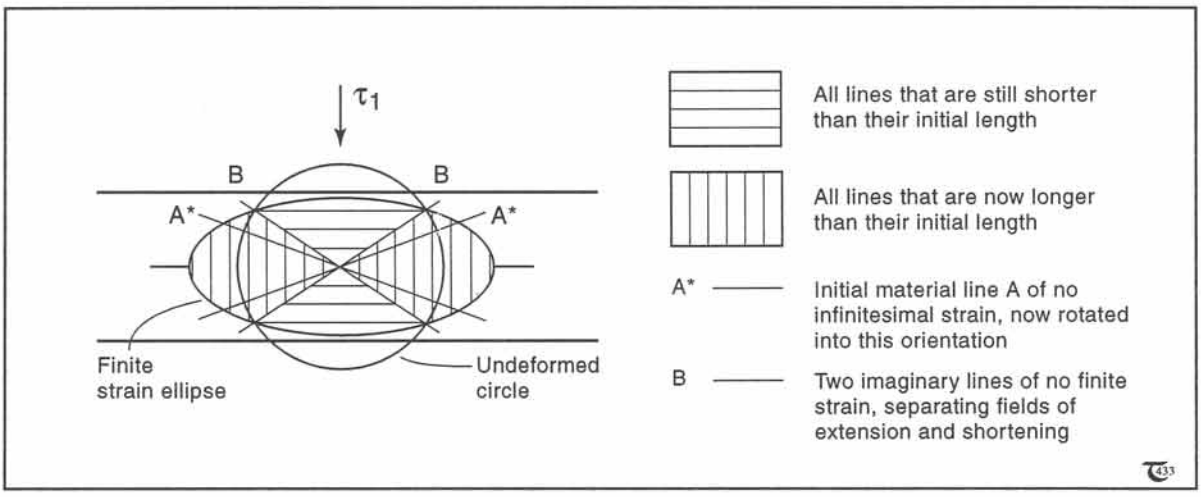

Figure 14-15: *Finite strain ellipse for pure shear deformation. See, also, Figure 14-9.*

14-5 Finite strain ellipse for pure shear

The superimposition of many strain increments results in a large or finite strain, graphically represented by a *finite strain ellipse*. Superimposition of the finite strain ellipse onto the undistorted strain circle yields four intersection points, connecting two diagonal lines which have lengths equal to that of the initial strain circle diameter (Fig. 14-15). These lines are imaginary *lines-of-no-finite-strain*, B, coinciding with material lines which have been shortening before and that will be swept into the extension field if another increment of strain is added. The rotation history of material lines, A^*, coinciding with the 45° lines-of-no-infinitesimal-strain at the onset of deformation, is included in the graph of Figure 14-11.

The orientation, α_B, of the imaginary lines, B, of no finite strain in *pure shear* at any particular stage of finite deformation is (using $S_1 = 1/S_3$ for isochoric plane strain):

$$\alpha_B = \tan^{-1}[(1-S_3^2)^{1/2}/(S_1^2-1)^{1/2}] = \tan^{-1}S_1^{-1} \quad (14\text{-}7)$$

The initial position of the material lines, B^*, that now became lines-of-no-finite-strain, B, is [combining equations (14-3a) and (14-7)]:

$$\alpha_{B^*} = \tan^{-1}[(S_1^4-S_1^2)^{1/2}/(S_3^2-S_3^4)^{1/2}] = \tan^{-1}[(S_1^8-S_1^6)^{1/2}/(S_1^2-1)^{1/2}] \quad (14\text{-}8)$$

Fi-gure 14-16 graphs the rotation history of the angles, α_B and α_{B^*}, versus S_1 for pure shear for S_1-values of 1 up to 6.

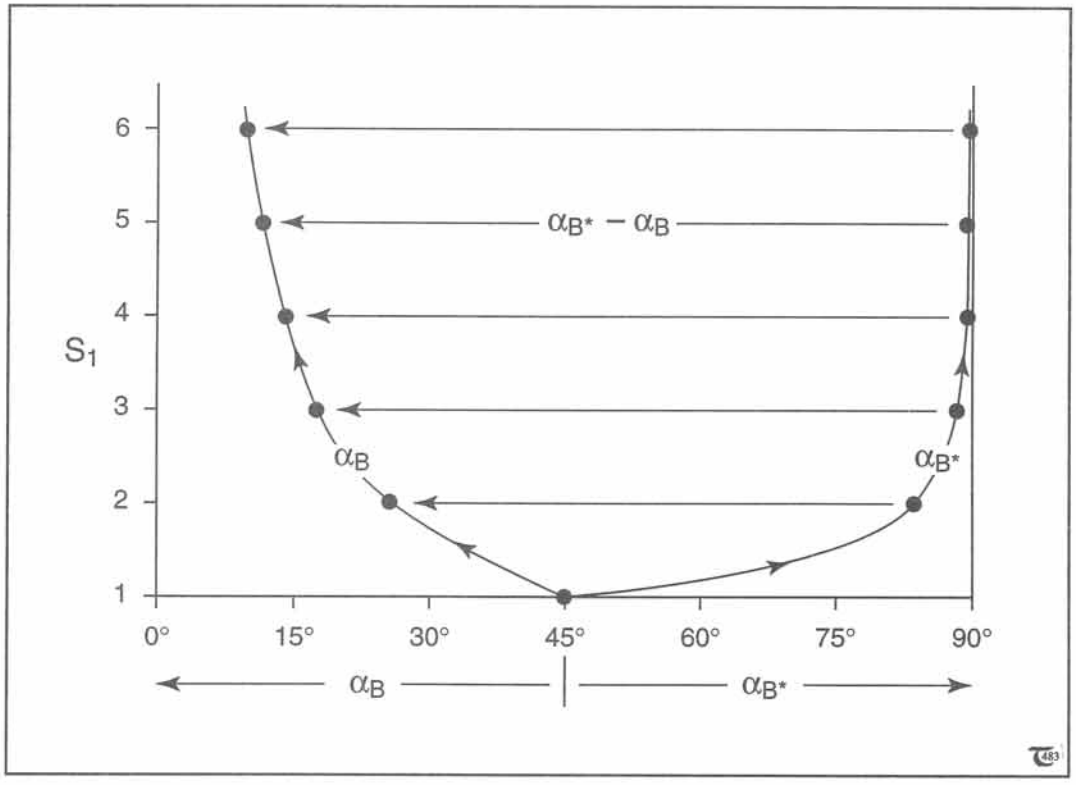

Figure 14-16: *Rotation history, α_B, for imaginary lines of no finite strain, B, and initial orientation, α_{B^*}, of material lines of no finite strain, B^*. Valid only for pure shear. See equations (14-7 & 14-8). The angle $(\alpha_{B^*}-\alpha_B)$ is the subject of exercise 14-10.*

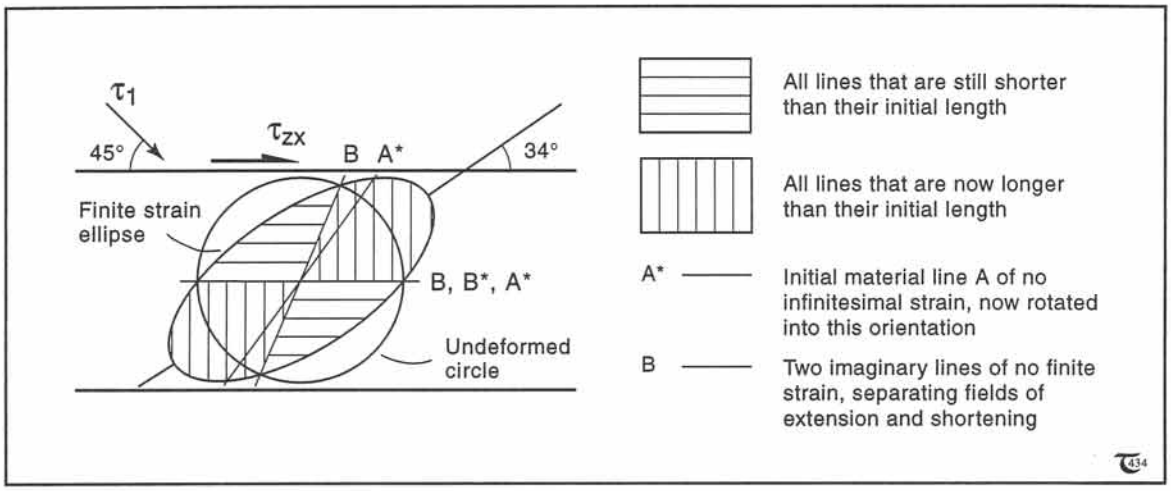

Figure 14-17: *Finite strain ellipse for simple shear deformation. See, also, Figure 14-12.*

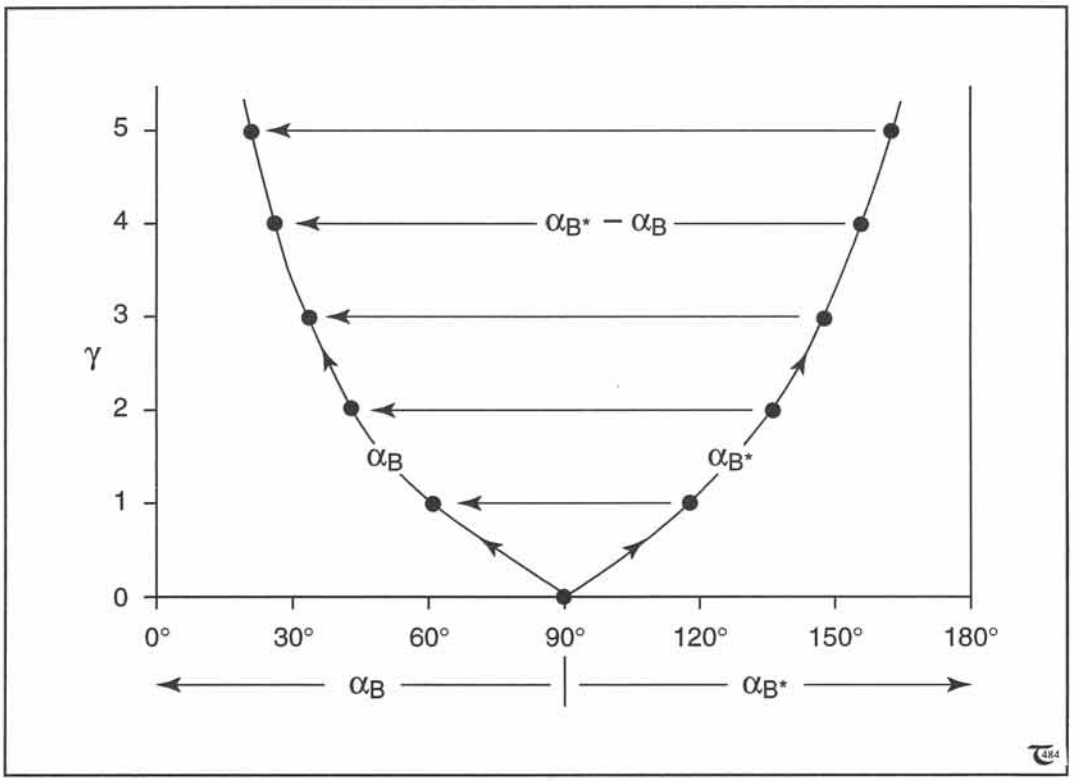

Figure 14-18: *Rotation history, α_B, for imaginary line of no finite strain, B, and initial orientation, α_{B^*}, of material line of no finite strain, B^*. Valid only for simple shear. See equations (14-9 & 14-10). The angle (α_{B^*}-α_B) is the subject of exercise 14-12.*

14-6 Finite strain ellipse for simple shear

The finite strain ellipse for *simple shear* deformation, is shown in Figure 14-17. The orientation of the imaginary line-of-no-finite-strain, B, can be obtained, combining equation (14-7) with an angle accounting for the rigid-body rotation of the strain ellipse, according to equation (12-8):

$$\alpha_B = \tan^{-1}S_1^{-1} + (1/2)\tan^{-1}(2/\gamma) \qquad (14\text{-}9)$$

with $S_1 = [(1/2)[\gamma^2+2+(\gamma^4+4\gamma^2)^{1/2}]]^{1/2}$, according to equation (12-7a). Note that one of the two lines, B, does not rotate at all and remains parallel to the direction of shear throughout the deformation.

The initial position of the material lines, B^*, that now became lines-of-no-finite-strain, B, follows from equation (14-5a):

$$\alpha_{B^*} = \tan^{-1}[(1/\tan\alpha_B)-\gamma]^{-1} \qquad (14\text{-}10)$$

with α_B computed from γ, according to equation (14-9). Figure 14-18 graphs the rotation history of the angles, α_B and α_{B^*}, against γ for simple shear deformation, for γ of 0 up to 5. Finally, the orientation, $\alpha_{S1,3}$, of the material lines, S_1 and S_3, before deformation is given by:

$$\alpha_{S1,3} = \tan^{-1}(2/\gamma) \qquad (14\text{-}11)$$

☐Exercise 14-11: Examine Figure 14-17. Color the ellipse sectors for finite shortening and extension, using colors different from those used in exercise 14-7a. Establish the finite strain in Figure 14-17, and check whether the lines, A^*, are in the appropriate orientation, using the graph of Figure 14-14.

☐Exercise 14-12: Plot a graph, showing the rotation history of the principal stretch axes with increasing angular shear strain, using equation (14-11).

☐Exercise 14-13: The angles $(\alpha_{B^*}-\alpha_B)$ indicated in Figure 14-18 measure the total rotation experienced by material lines that become lines of no finite strain. a) Produce a separate graph of $(\alpha_{B^*}-\alpha_B)$ versus S_1. b) Explain the implication of this plot for the volume of rock still not shortened after a principal stretch of 6.

14-7 Strain history ellipse

The infinitesimal and finite strain ellipses can be superimposed simultaneously onto the undistorted strain circle. This superimposition ellipse is coined here the *strain history ellipse*, in which four different types of segments can be distinguished, each containing material lines with a common distortion history (Figs. 14-19a & b). *Type 1 segments* comprise material lines, which have only been shortened. *Type 2 segments* comprise material lines, which have initially shortened, but that are now extending again, while their overall lengths are still shorter than their initial length. *Type 3 segments* contain lines that initially shortened, but that are now already extended beyond their initial length. *Type 4 segments* contain lines that have never shortened and that are only extending.

Competent single layers embedded in incompetent rock display a variety of structures if deformed by shortening or stretching: folds, boudins, or pinch-and-swells. The four segments in each of the strain history ellipses of Figures 14-19a & b, if containing *competent single layers*,

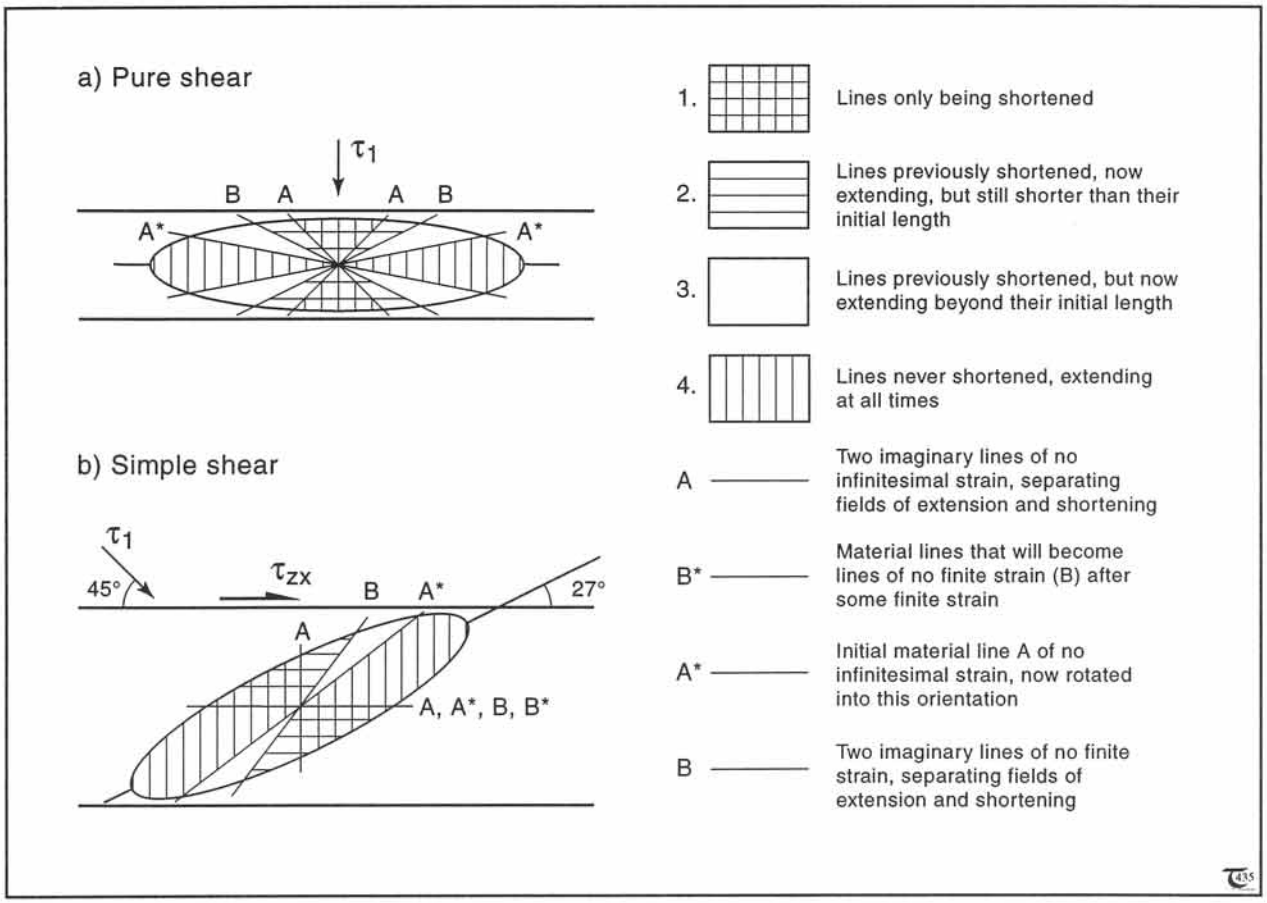

Figure 14-19: *a) & b) Ellipse of superimposed strain histories (incremental and finite) for pure and simple shear deformation.*

will contain: material layers only shortened into folds (*segments 1*); layers only extended by necking into boudins or pinch-and-swells (*segments 4*); layers first shortened into folds that are now being unfolded (*segments 2*); or layers that have already been stretched beyond their initial length into boudins and pinch-and-swells (*segments 3*).

Incompetent single layers hosted by more *competent matrix rock* may develop mullions and inverse folds (Fig. 14-20). Mullions form in incompetent layers that are parallel to the shortening direction (Fig. 14-21). Inverse folds are thought to look similar to pinch-and-swells, but it must be emphasized that inverse folds are rare and most incompetent layers are likely to extend uniformly.

The four segments of Figures 14-19a & b, if containing *incompetent single layers*, will contain: material lines only shortened into mullions (*segments 1*); layers only extended uniformly into inverse folds (*segments 4*); layers first shortened into mullions that may open by layer-parallel extension (*segments 2*); or layers that have already been stretched beyond their initial length into inverse folds (*segments 3*).

The strain history ellipse considers only the change in length and orientation of *passive* marker lines. The detailed mechanical interaction between a single layer and the ambient rock is not taken into account. Nonetheless, this simple geometrical approach predicts results in agreement with dynamically scaled models of the formation of mullions, boudins, and folds.

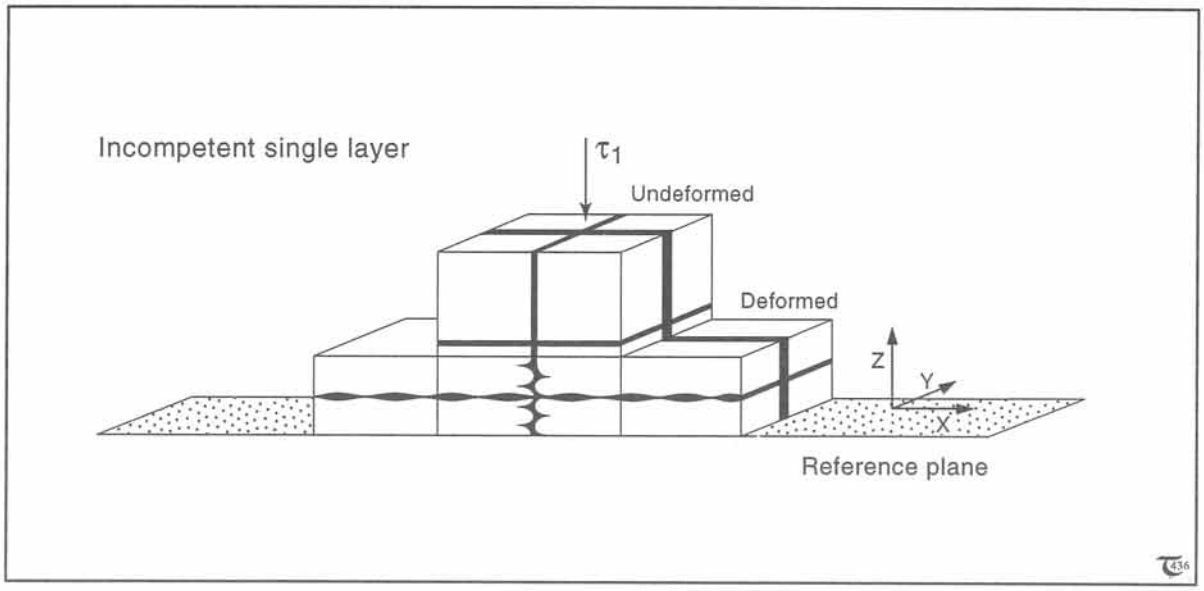

Figure 14-20: *The orientation of mullions and inverse folds of incompetent single layers with respect to the directions of shortening and extension.*

Figure 14-21: *Mullions of incompetent pelitic schist layer, shortened inside metasandstones of Loch Monar, Inverness-shire, Scotland. Courtesy John Ramsay.*

14-8 Dome-and-basin folds and chocolate-tablet boudinage

Competent single layers embedded in incompetent rock may develop a variety of structures if deformed by shortening or stretching in the ductile field. Figures 14-24a to d illustrate qualitatively the orientation of buckling and boudinaging of competent single layers, initially coinciding with the principal planes containing the ellipsoid axes S_1, S_2, and S_3. The three planes considered contain the largest or smallest bulk shortening or extension, or both. Any competent layer, containing the long axis of the strain ellipsoid, will boudinage by stretch in the S_1-direction and simultaneously fold in the direction perpendicular to S_1, due to coeval shortening.

Dome-and-basin folds characteristically form in prolate deformations and imply that the major axis of the strain ellipsoid (S_1) is perpendicular to the enveloping surface of the folds (Fig. 14-24c). *Chocolate-tablet boudinage* is characteristic for oblate deformations and implies that the minor axis of the strain ellipsoid (S_3) is perpendicular to the boudinaged tablets (Fig. 14-24d). *Uni-directional boudins* in straight layers and *non-stretched fold axes* uniquely occur in plane strain deformation.

Prolate and oblate coaxial deformations of competent single layers of arbitrary orientation are less complex than that of plane deformation. This is because coaxial prolate and oblate deformations both possess an axis of symmetry. Prolate deformations are radially symmetric about the S_1-axis, so that any competent layers, containing the S_1-axis, will fold and boudinage without rotation of the enveloping surface (Fig. 14-24c). Oblate deformations are symmetric about the S_3-axis, so that any competent layers, containing the S_3-axis, will fold and boudinage without rotation

□Exercise 14-14: Figure 14-22 is the finite strain ellipse for a pure shear deformation of stretch $S_1=1.5$. a) Convert this finite strain ellipse into a strain history ellipse, indicating the lines, A and B, in the appropriate orientation, by superposing the undistorted unit circle and the incremental strain ellipse. b) Check the angle, α_B, found in the construction, with values from the graph for pure shear, plotted in Figure 14-16. c) Complete the strain history ellipse by including the orientation of line A*, using the graph of Figure 14-11. d) Indicate in which sectors folds, mullions, and boudins may occur.

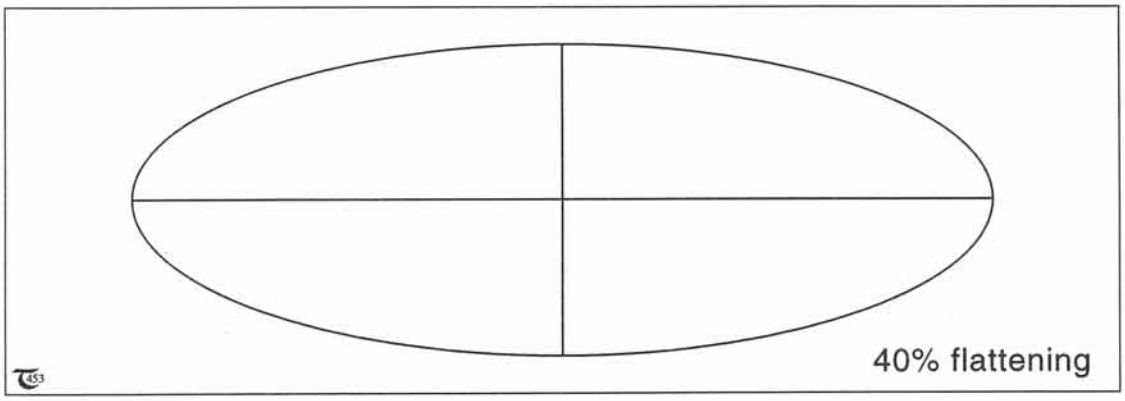

Figure 14-22: *Finite strain ellipse for a pure shear with major principal stretch of 1.5. Template for exercise 14-14.*

of the enveloping surface (Fig. 14-24d). Any plane containing the S_1-axis in prolate strain and any plane containing the S_3-axis in oblate strain will automatically contain a second principal strain axis, due to radial symmetry. However, plane strain deformation lacks such a radial symmetry axis (Fig. 14-24b). Consequently, *plane strain is more complex than both oblate and prolate strains*, especially if the progressive deformation of material planes of arbitrary orientation is considered.

The layers in Figures 14-24a to d summarize all *non-rotational deformations* of single layers in coaxial bulk deformation. Fold limbs may rotate if tightly folded, but their enveloping surfaces remain parallel to the initial layer and coincide with the principal planes of the strain ellipsoid. The enveloping surface of a folding or boudinaging layer remains stationary only if the competent layer is initially parallel to any plane containing at least two of the principal axes of

☐Exercise 14-15: Figure 14-23 is the finite strain ellipse for a unit simple shear deformation ($\gamma=1$). a) Convert this finite strain ellipse into a strain history ellipse, indicating the lines, A and B, in the appropriate orientation, by superimposing the undistorted unit circle and the incremental strain ellipse. b) Check the angle, α_B, found in the construction, with values from the graph for simple shear, plotted in Figure 14-18. c) Complete the strain history ellipse by including the orientation of line A*, using the graph of Figure 14-14. d) Indicate in which sectors folds, mullions, and boudins may occur.

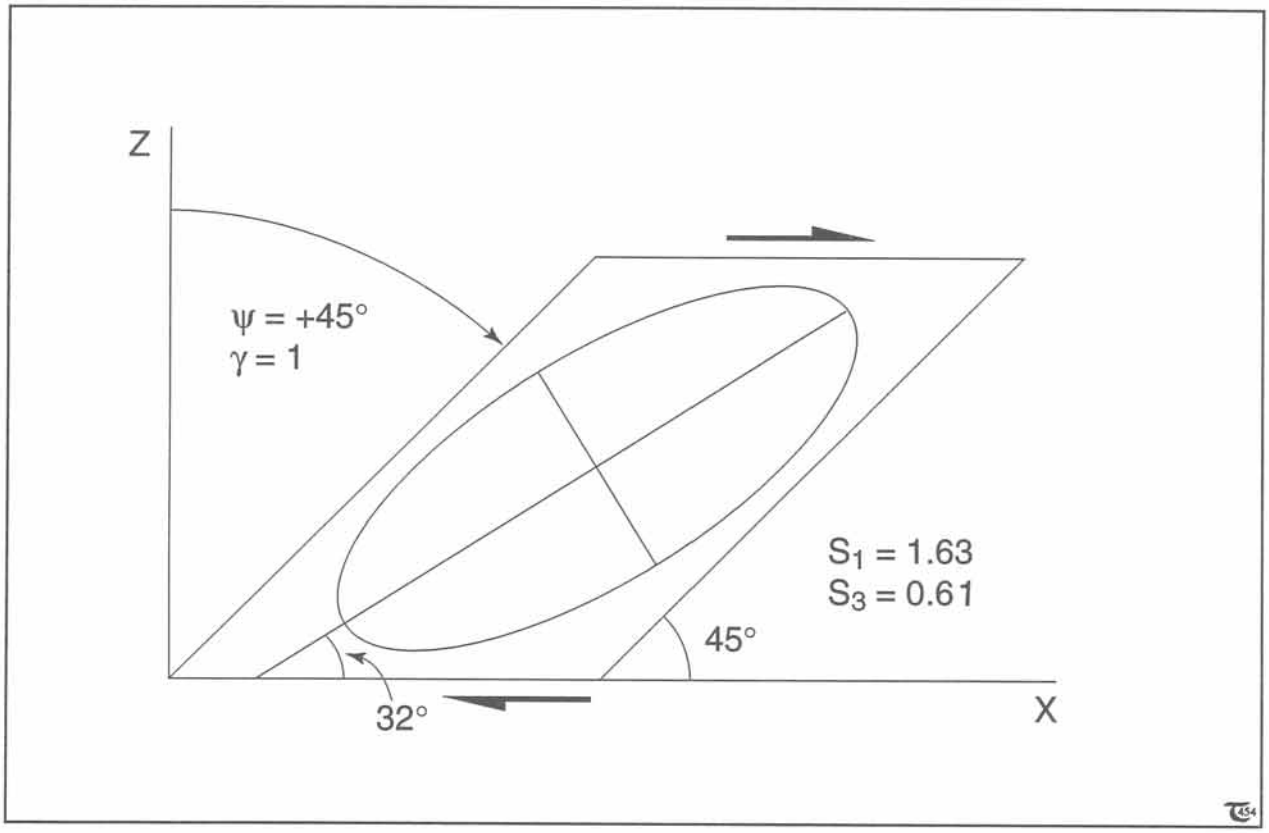

Figure 14-23: Finite strain ellipse for unit simple shear. Template for exercise 14-15.

strain (Figs. 14-24a to d). The progressive deformation of competent single layers in coaxial bulk deformation evolves not necessarily without rotation. Competent single layers, which do not coincide with any of the principal planes of the bulk strain ellipsoid, will always *rotate* towards the extension direction, even in coaxial deformation.

Deformed competent single layers may, also, contribute to constrain the finite strain ellipsoid. The occurrence of *dome-and-basin folds* is char-

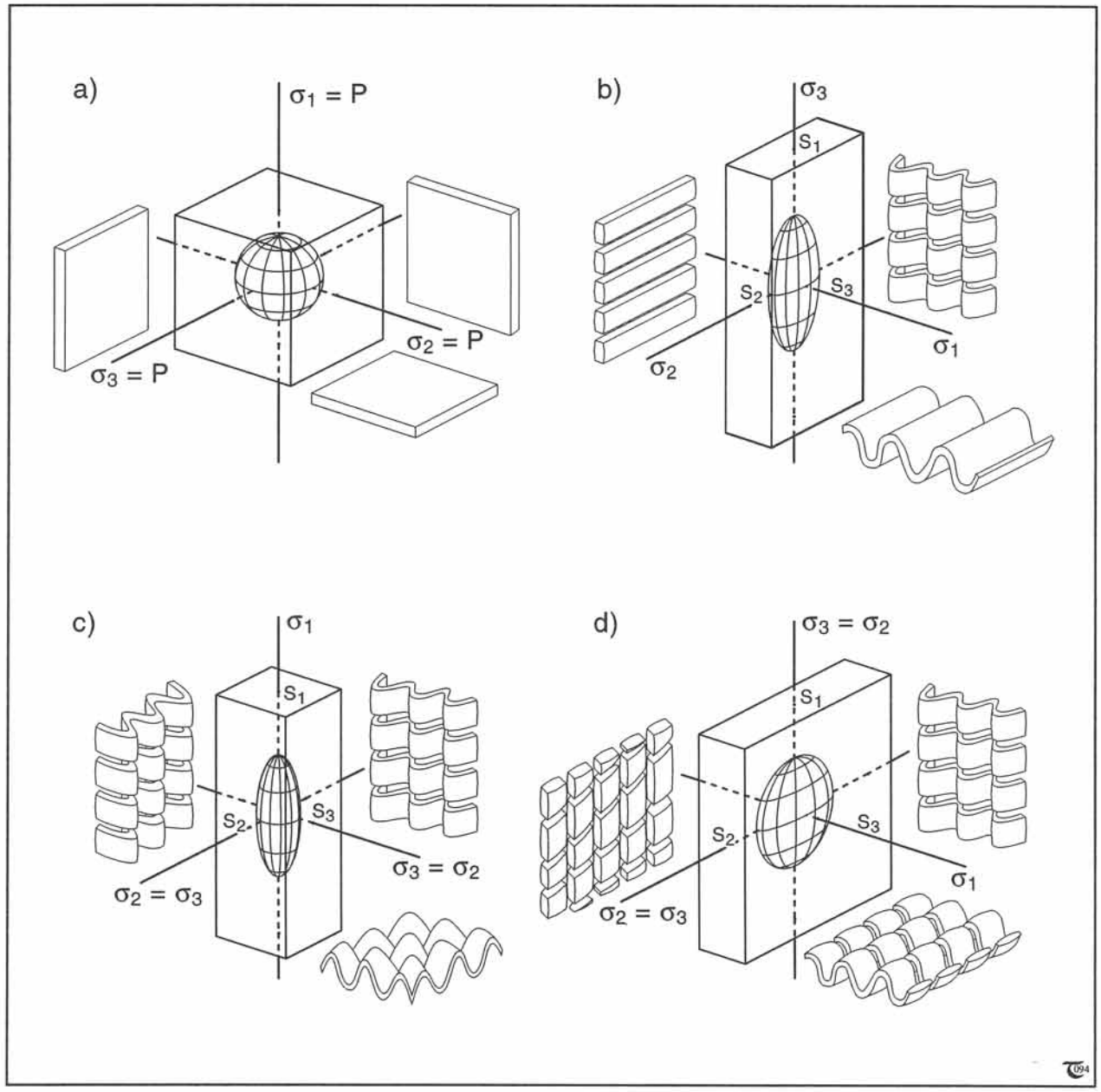

Figure 14-24: *a) to d) Buckling and boudinaging of competent single layers, initially coinciding with the principal planes, containing the ellipsoid axes, S_1, S_2, and S_3. Illustrated are: (a) the undeformed unit sphere, (b) plane strain, (c) prolate strain, and (d) oblate strain.*

☐**Exercise 14-16: This section considered what deformation structures may form in *competent* single layers, coinciding with the principal planes of the three principal types of strain ellipsoids. Figure 14-25a to d illustrates what would happen to an *incompetent* single layer. Explain the various structures.**

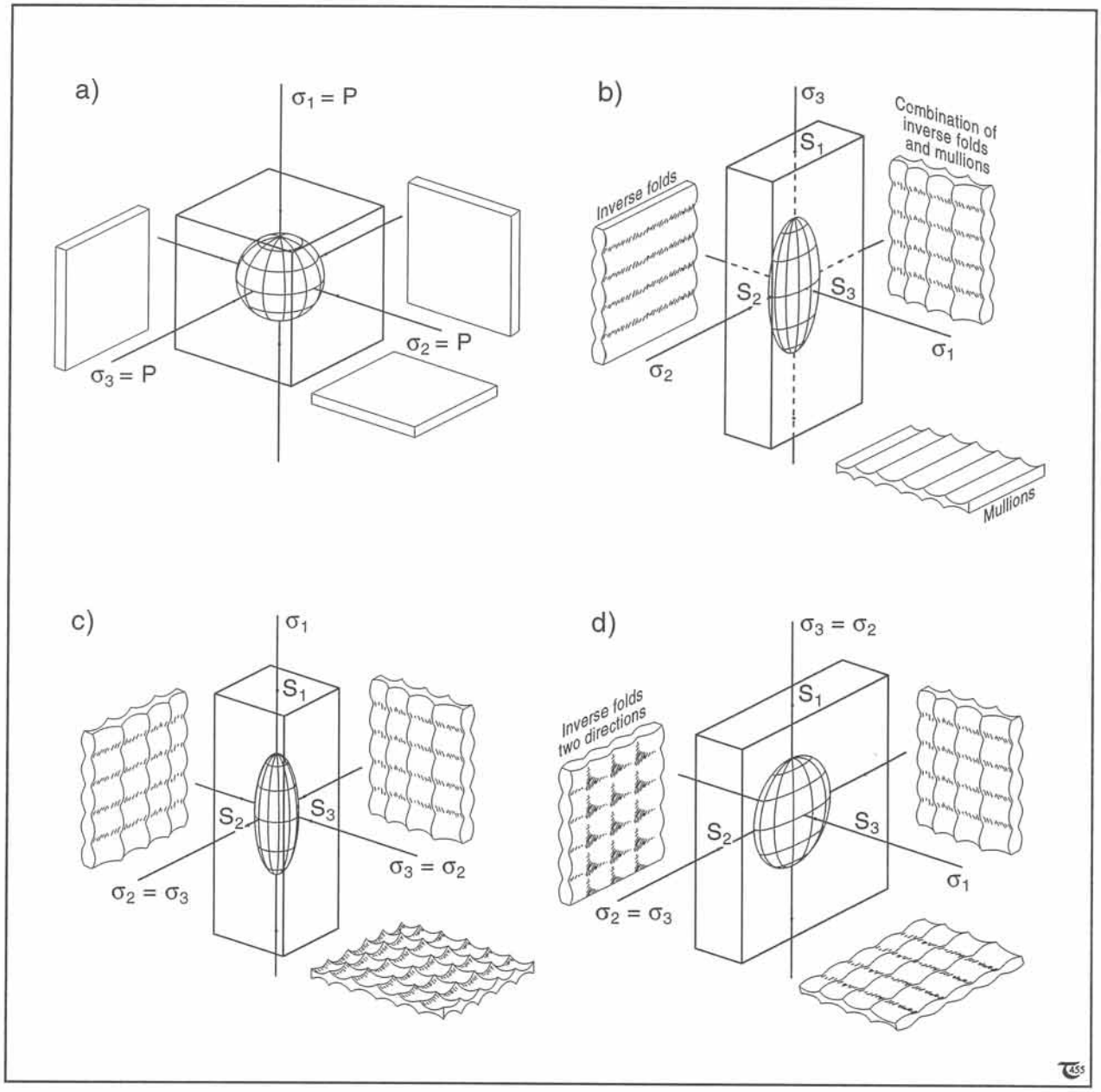

Figure 14-25: *a) to d) Mullioning and inverse folding of incompetent single layer, coinciding with the principal plane of strain, is indicated. Illustrated are (a) the undeformed unit sphere, (b) plane strain, (c) prolate strain, and (d) oblate strain.*

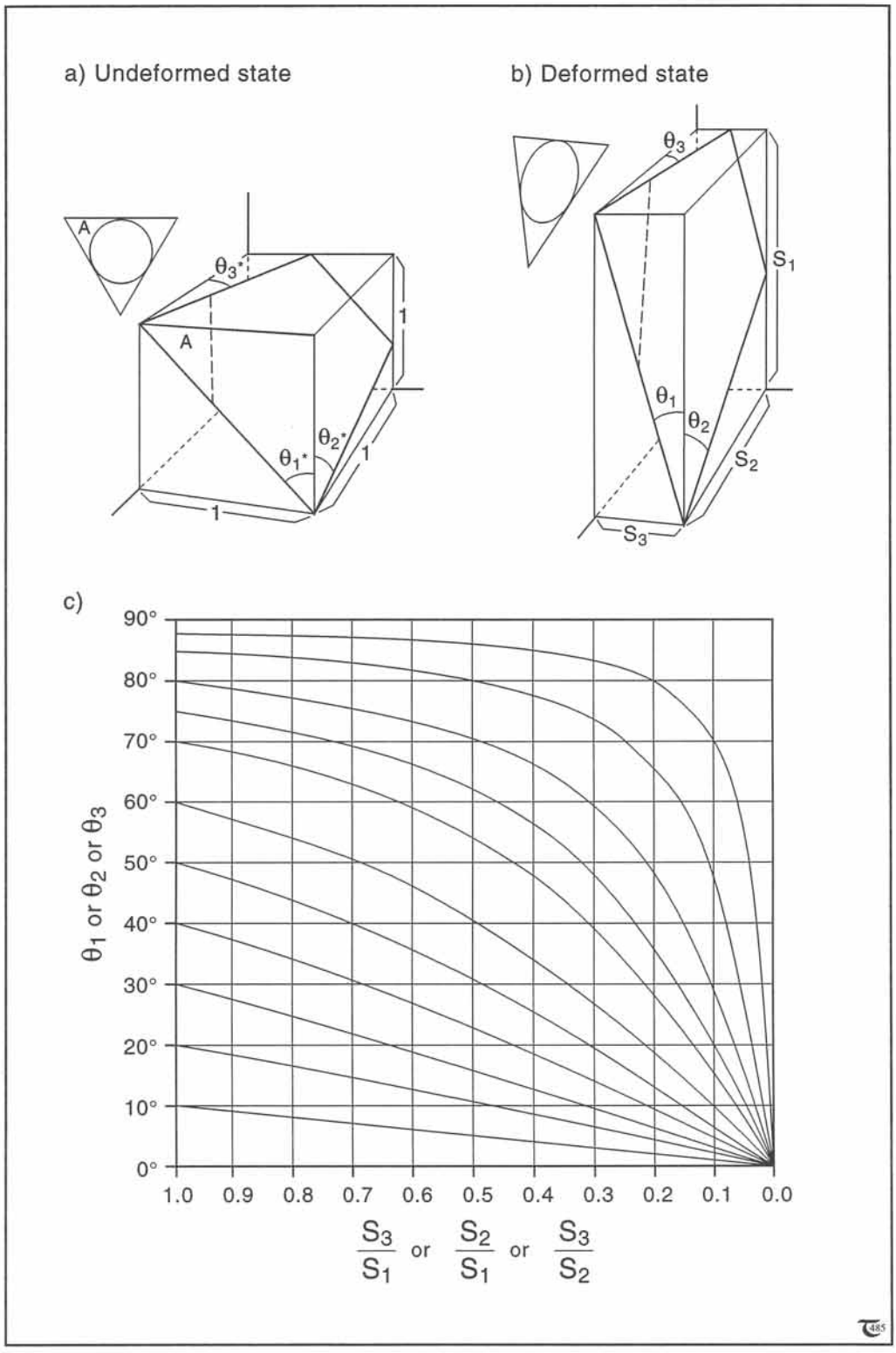
a) Undeformed state
b) Deformed state
A
A
θ_3^*
θ_2^*
θ_1^*
1
1
1
θ_3
S_1
θ_1
θ_2
S_2
S_3
c)
90°
80°
70°
60°
50°
40°
30°
20°
10°
0°
θ_1 or θ_2 or θ_3
1.0 0.9 0.8 0.7 0.6 0.5 0.4 0.3 0.2 0.1 0.0
$\frac{S_3}{S_1}$ or $\frac{S_2}{S_1}$ or $\frac{S_3}{S_2}$

Figure 14-26a to c: (a & b) Undeformed and deformed states of a unit cube, containing an arbitrary plane, A, with direction cosines as shown. The angles in undeformed state are asterisked. (c) The angles, θ_1, θ_2, and θ_3, fixing the orientation of plane A, are graphed versus finite stretch ratios (S_3/S_1, S_2/S_1, or S_3/S_2). See equations (14-12a to c).

acteristic for prolate deformations and fixes the orientation of the major axis of the strain ellipsoid, S_1, perpendicular to the enveloping surface of the folds. The occurrence of *chocolate-tablet boudinage* is characteristic for oblate deformations and fixes the orientation of the minor principal strain axis, S_3, perpendicular to the enveloping surface of the tablet. *Uni-directional boudins* in straight layers and *non-stretched fold axes* uniquely occur in plane strain deformation. The orientation of three ellipsoid axes may be constrained, using either a boudinaged layer or a folded layer, or both. All these conclusions assume that the field structures of concern have formed in a single deformation phase. For example, dome-and-basin folds and chocolate-tablet boudinage may, also, form by superimposing multiple deformation phases at right angles.

14-9 Rotation of lines and planes in 3D coaxial deformation

The change in orientation of a plane in 3D deformation is easy to compute if the three principal stretches, S_1, S_2, and S_3, are known. The initial orientation of an arbitrary plane, A, can be specified in terms of three angles, θ_{1*}, θ_{2*}, and θ_{3*}, as defined in Figure 14-26a. These angles will change into angles θ_1, θ_2, and θ_3 after some finite strain (Fig. 14-26b); following from:

$$(\tan\theta_1/\tan\theta_{1*}) = S_3/S_1 \qquad (14\text{-}12a)$$
$$(\tan\theta_2/\tan\theta_{2*}) = S_2/S_1 \qquad (14\text{-}12b)$$
$$(\tan\theta_3/\tan\theta_{3*}) = S_3/S_2 \qquad (14\text{-}12c)$$

The decrease of angles θ_1, θ_2, and θ_3 with increasing strain is plotted in Figure 14-26c. In field

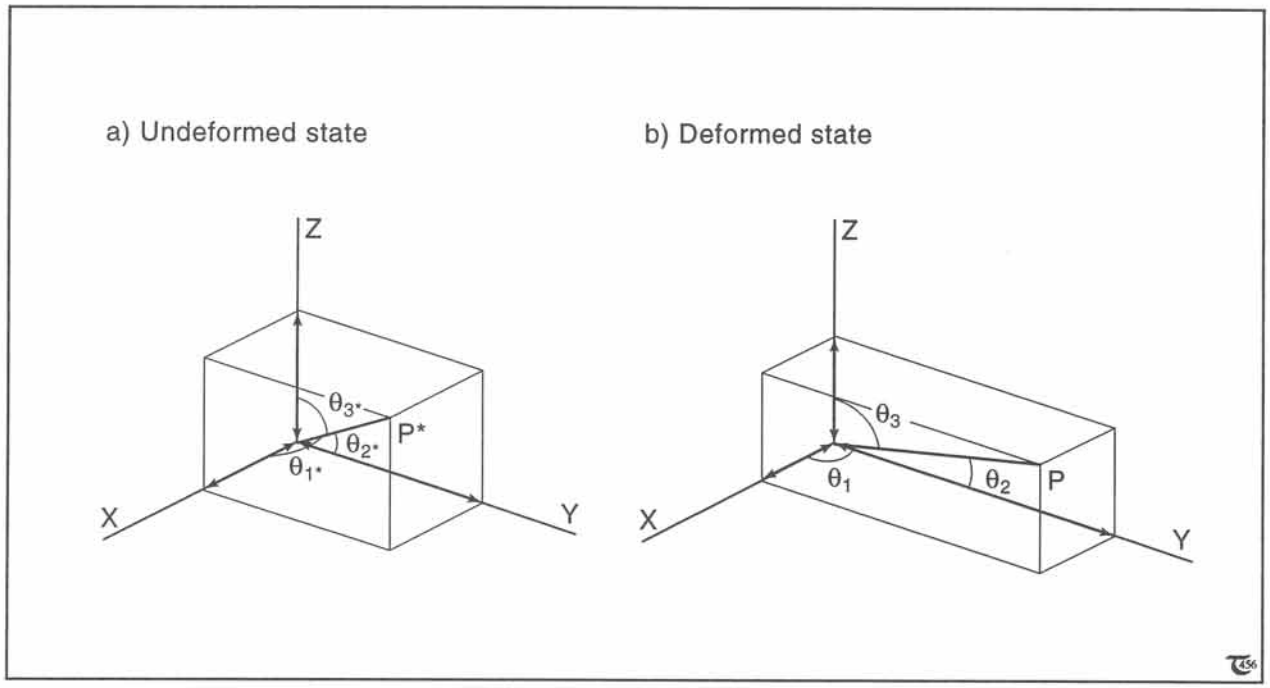

Figure 14-27: a) & b) Undeformed and deformed states of a rectangle, containing line OP. The orientation of the line is fixed by θ_1, θ_2, and θ_3. Original angles are asterisked.

assessments, the initial angles, θ_{1*}, θ_{2*}, and θ_{3*}, can be estimated from the graph in Figure 14-26c, if both the stretches (S_1,S_2,S_3) and final orientations $(\theta_1,\theta_2,\theta_3)$ have been determined for a particular plane. The final angles all approach zero for infinitely large strain, when S_3, also, vanishes.

The stretch, S_{OP}, undergone by an arbitrary line, OP (Fig. 14-27a & b), can, also, be calculated if both the stretches (S_1,S_2,S_3) and final orientations of the direction cosines angles $(\theta_1,\theta_2,\theta_3)$ are known:

$$S_{OP}=(S_1^2\cos^2\theta_1+S_2^2\cos^2\theta_2+S_3^2\cos^2\theta_3)^{1/2} \quad (14\text{-}13)$$

The initial orientation of the material line, OP, is given by $(\theta_{1*},\theta_{2*})$(Fig. 14-27a):

$$\cos^2\theta_{1*}=S_1^2\cos^2\theta_1/[\cos^2\theta_1(S_1^2-S_3^2)+\cos^2\theta_2(S_2^2-S_3^2)] \quad (14\text{-}14a)$$
$$\cos^2\theta_{2*}=S_2^2\cos^2\theta_2/[\cos^2\theta_1(S_1^2-S_3^2)+\cos^2\theta_2(S_2^2-S_3^2)] \quad (14\text{-}14b)$$

☐Exercise 14-17: For pure shear without any volume change, equations (14-12a to c) simplify. a) Write the simplified set of equations. b) Use Figure 14-26c to obtain the initial orientation $(\theta_{1*},\theta_{2*},\theta_{3*})$ of a plane, which has orientation $(\theta_1,\theta_2,\theta_3)=$ $(10°,30°,10°)$ after a pure shear of stretch, $S_1=2$. c) Sketch the plane within the deformed rectangular prism and the initial, undeformed cube.

☐Exercise 14-18: Consider a bulk pure shear deformation with shortening in the Z- and extension in the X-directions (Fig. 14-27b). Calculate the stretch of lines with the following direction cosines angles $(\theta_1,\theta_2,\theta_3)$ after the deformation: a) $(90°,90°,0°)$, b) $(90°,0°,90°)$, c) $(0°,90°,90°)$, and d) $(90°,30°,60°)$.

14-10 Surface-of-no-finite-strain in 3D

In 3D deformation, regions in which lines are shortening and extending are separated by the surface-of-no-finite-strain (SNFS). The lines that make up these surfaces are found by intersecting the undistorted strain sphere with the finite strain ellipsoid. Figures 14-28a to d illustrate the coaxial distortion of a unit sphere inside a unit cube into plane strain, prolate, and oblate ellipsoids. For the undeformed sphere, the SNFS is any plane through the center of the sphere (Fig. 14-28a).

For *plane strain*, the SNFS is found in two conjugate planes, intersecting in the S_2-axis (Fig. 14-28b). In the S_1-S_2-plane, all lines have extended, except for lines which are parallel to the S_2-axis. Reversely, all lines within the S_2-S_3-plane have shortened, except for lines which are parallel to the S_2-axis. Finally, sections parallel to the S_1-S_3-plane contain sectors with lines that shortened, separated by sectors with extending lines. The SNFS are imaginary surfaces, through which material lines will rotate during progressive deformation, so as to asymptotically approach the orientation of the maximum finite stretch. The area of the sector of extension will decrease with increasing magnitude of the finite strain.

For *prolate deformation*, the SNFS is a cone with an angle less than 45° (Fig. 14-28c). Typically, all lines within the S_2-S_3-plane have shortened. Any section parallel to the S_1-axis will contain sectors with lines that shortened, separated by sectors with extending lines. For *oblate deformation*, the SNFS is, also, a cone, but with a cone angle larger than 45° (Fig. 14-28d). Typically, all lines within the S_1-S_2-S_3-plane have extended. Any section parallel to the S_3-axis will contain sectors with lines that shortened, separated by sectors with extending lines. The area of the sector of extension will decrease with increasing magnitude of the finite strain.

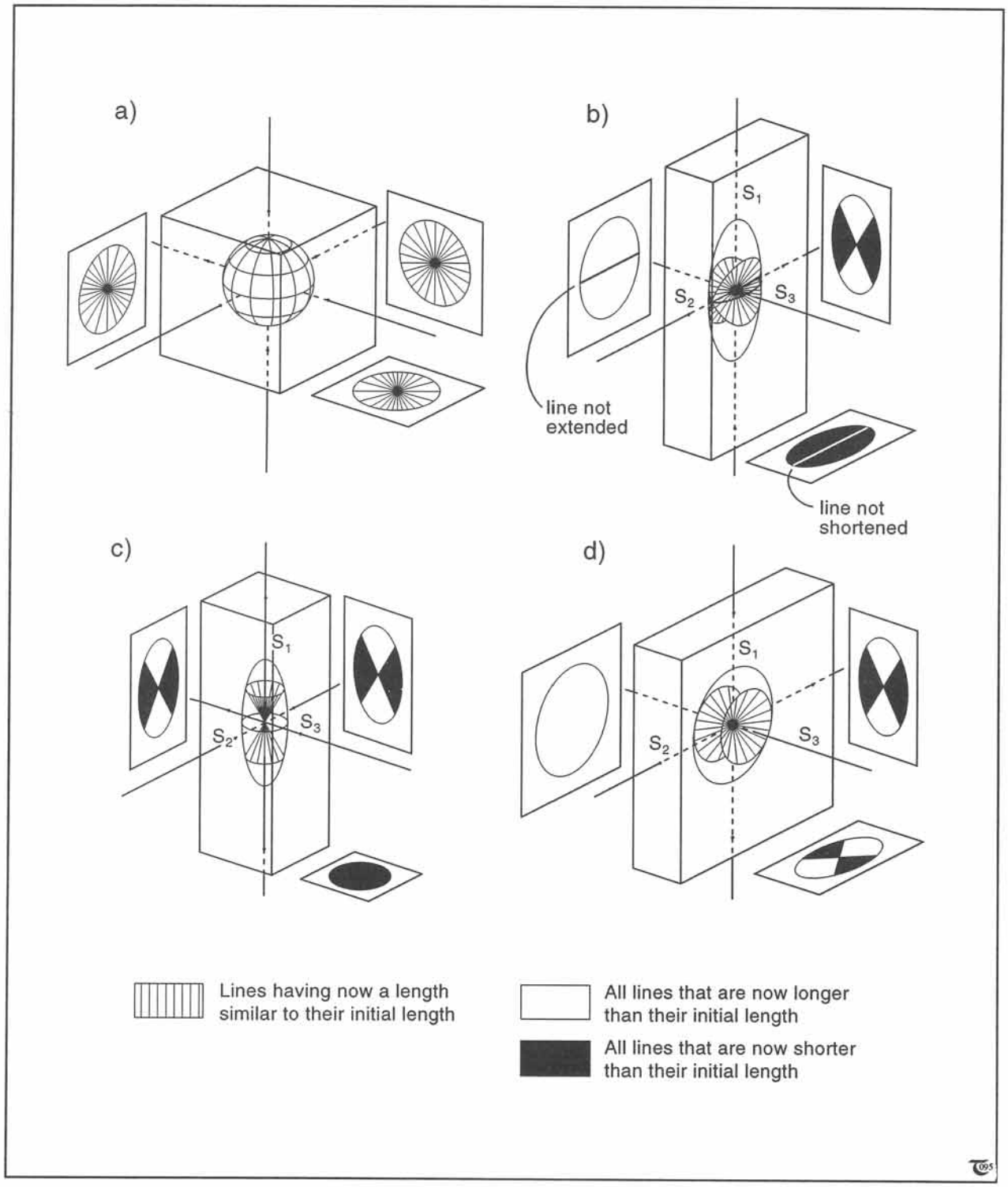

Figure 14-28: *a) to d) Shape and principal sections of the surface-of-no-finite-elongation (SNFE) for: (a) undeformed sphere, (b) plane strain, (c) prolate strain, and (d) oblate strain.*

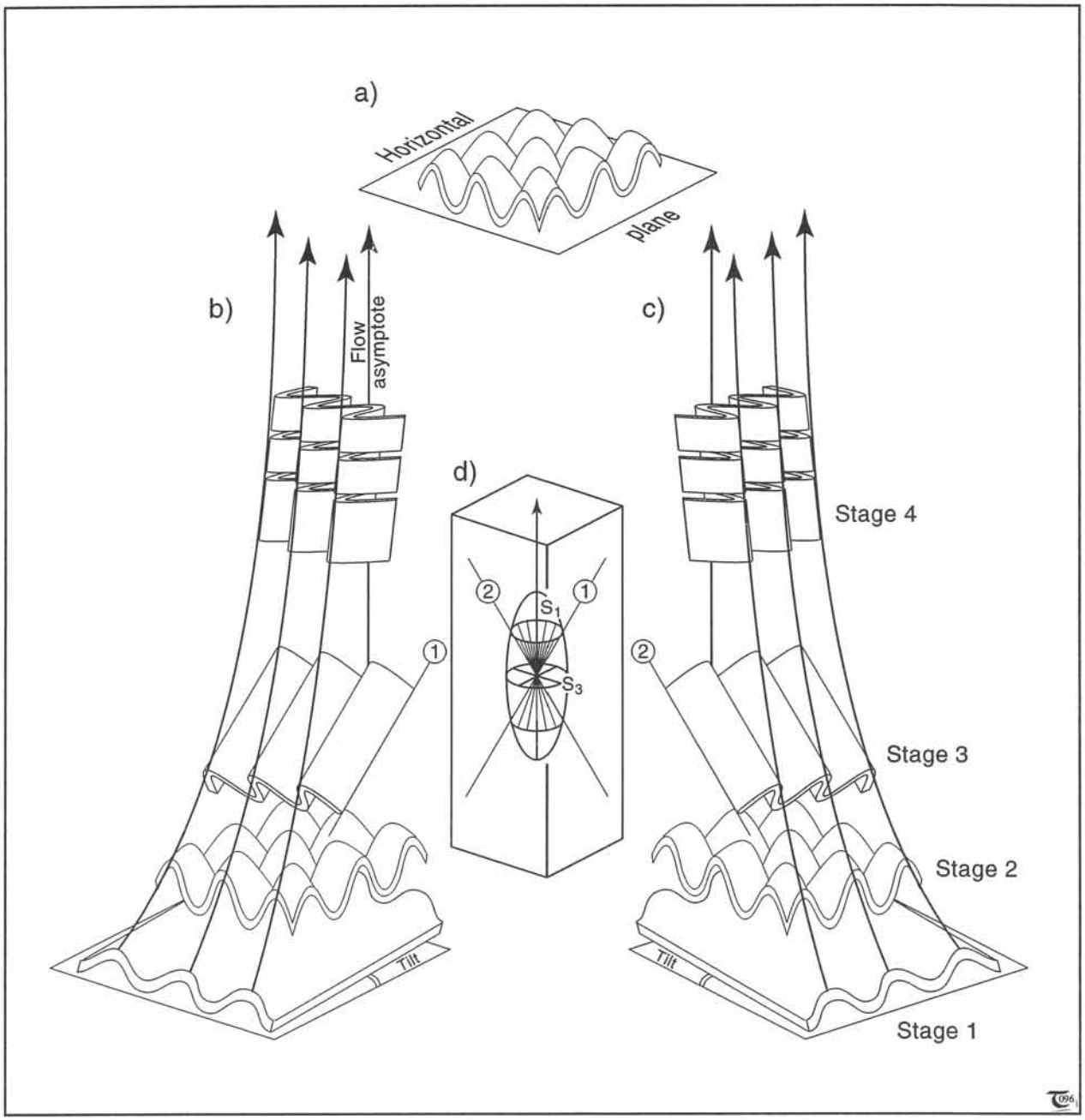

Figure 14-29: *a) to d) Progressive deformation of single competent layers in coaxial prolate strain. (a) Layers coinciding with the S_2-S_3-plane of maximum constriction will not rotate during progressive shortening but will deform and amplify a pattern of dome-and-basin folds. (b & c) Layers inclined to the plane of maximum constriction will rotate progressively and deform (shown are 4 stages), while travelling along the streamlines towards the extensional flow asymptote parallel to the ellipsoid's S_1-axis. The fold axes perpendicular to the S_1-axis will unfold and material lines will have resumed their initially straight orientation (stage 3), when rotating into parallelism with the particular lines (labeled 1 and 2) of (d), the cone-of-no-finite-elongation.*

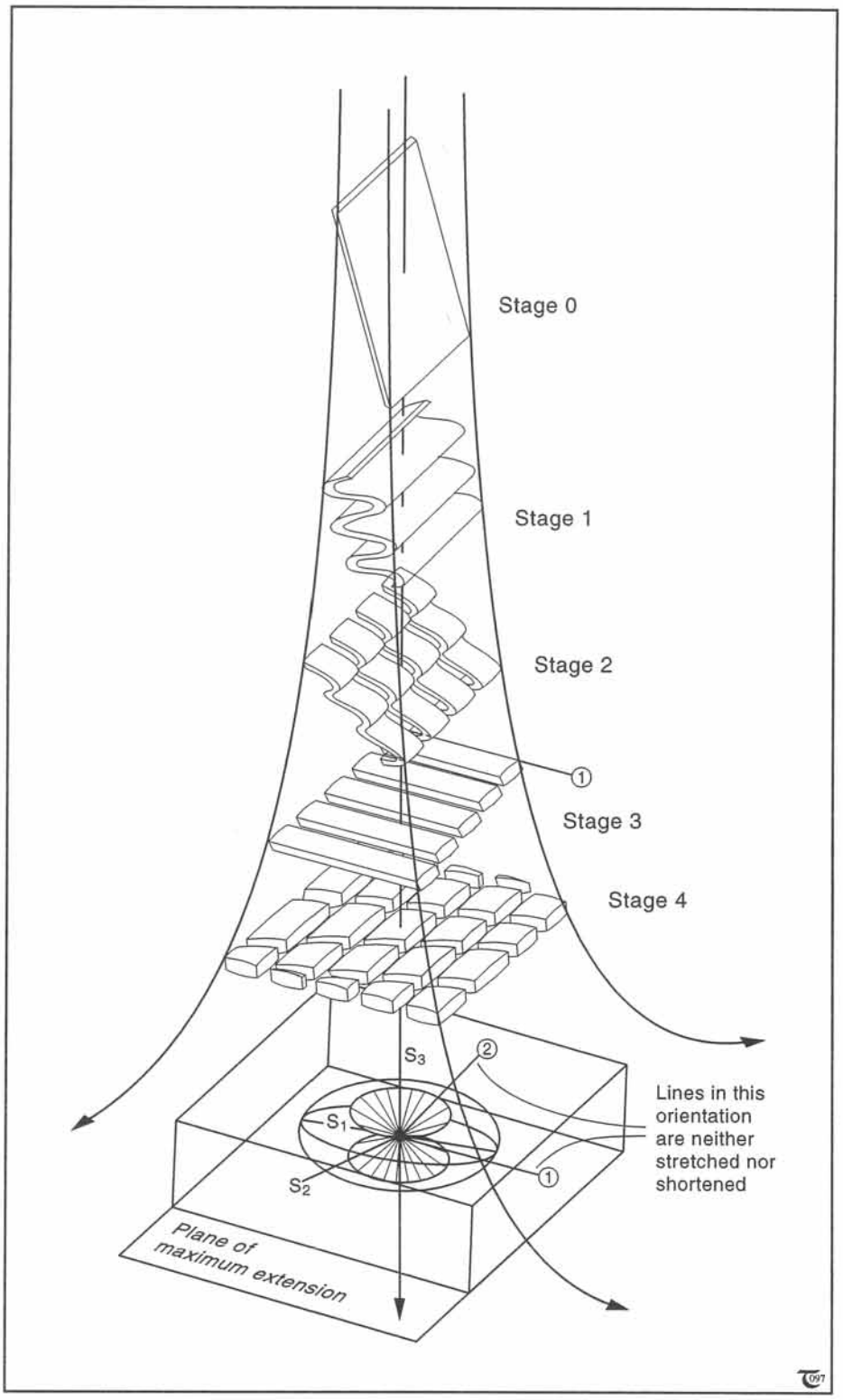

Figure 14-30: *Progressive deformation of single competent layers in coaxial oblate strain. Layers coinciding with the S_1-S_2-plane of maximum extension will not rotate during progressive shortening but develop a pattern known as chocolate-tablet boudinage. All other layers, initially inclined to the plane of maximum extension, will progressively rotate and deform (shown are 4 stages), while traveling along the streamlines towards the S_1-S_2-plane of extensional flow. The fold axes, perpendicular to the S_3-axis, unfold and material lines, perpendicular to the fold axis, resume their initially straight orientation (stage 3), when rotated into parallelism with any of the lines (e.g., those labeled 1 and 2), making up the cone-of-no-finite-elongation.*

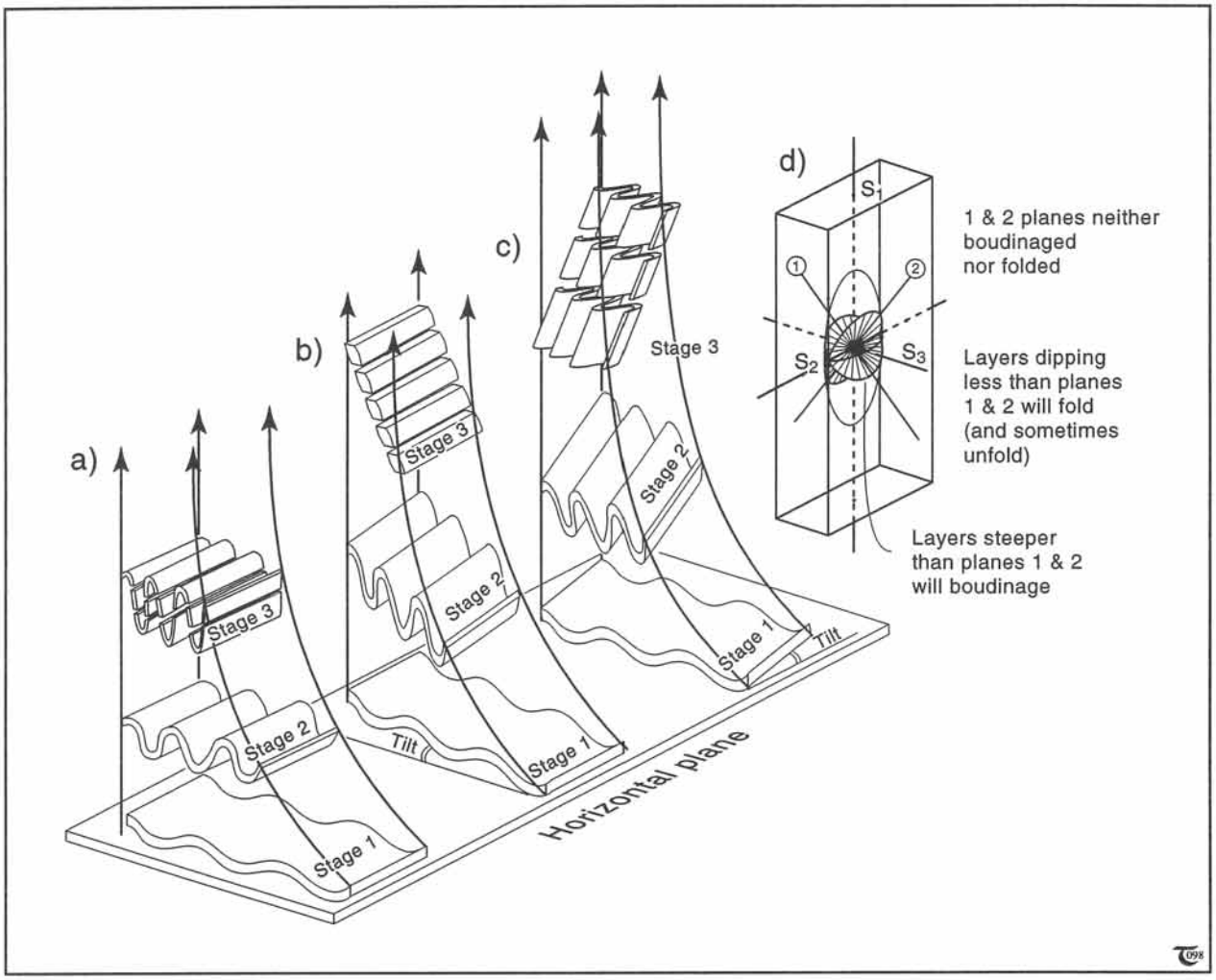

Figure 14-31: *a) to d) Progressive deformation of competent single layers in coaxial plane deformation. The extensional flow asymptotes are all parallel to the S_1-S_2-plane of the strain ellipsoid. (a) Layers initially in the S_2-S_3-plane fold about axes, parallel to the S_2-axis at all times. The enveloping surface of minor folds will not rotate, but their limbs may stretch into boudins if steeper than the planes-of-no-finite-elongation. (b) Layers, comprising the b-axis but initially inclined to the S_3-axis, will first fold but then unfold, while rotating towards parallelism with the extensional flow asymptote (S_1-axis). Material lines will have resumed their initially straight orientation (between stages 2 and 3), when rotated into parallelism with any of the lines, making up the plane-of-no-finite-elongation. (c) Layers, comprising the S_3-axis but initially inclined to the S_2-axis, will first fold but then unfold, while rotating towards parallelism with the extensional flow asymptote (S_1-axis). (d) Plane strain ellipsoid.*

☐Exercise 14-19: Compare Figures 14-28a to d with 14-24a to d. a) Explain why unidirectional boudins in straight layers, single folds, chocolate-tablet boudinage, and dome-and-basin folds are all unique for a particular orientation with a particular shape of the strain ellipsoid. b) Explain why it is impossible to constrain the direction of the separation channels of chocolate-tablet boudinage in perfect oblate strain. c) Explain why it is impossible to predict the orientation of the egg-carton grooves of dome-and-basin folds in perfect prolate strain.

14-11 Deformation of single layers in 3D

Competent single layers, not coinciding with any of the principal planes of the bulk strain ellipsoid, will always *rotate* towards the extension direction, even in coaxial deformation. Layers which contain the maximum shortening axis, but which are inclined to the ellipsoid's other two axes, will initially shorten, but may eventually extend into boudins. The progressive deformation of such layers can be understood by considering the *surface-of-no-finite-strain* (SNFS), found by intersecting the finite strain ellipsoid with the undeformed unit sphere.

Prolate and oblate coaxial deformation of competent single layers of arbitrary orientation is less complex than that of plane deformation and is, therefore, discussed first. Figures 14-29a to d summarize the progressive deformation of competent single layers in *coaxial prolate strain*. Layers, coinciding with the S_2-S_3 plane of maximum constriction, will not rotate during progressive shortening but will deform and amplify a pattern of dome-and-basin folds (Fig. 14-29a). Layers, inclined to the plane of maximum constriction, will rotate progressively towards the maximum extension direction, parallel to the strain ellipsoid's S_1-axis (Figs. 14-29b & c). The fold axes perpendicular to the S_1-axis will unfold, and material lines will have resumed their intially straight orientation (*stage 3*) when rotating into parallelism with any of the lines making up the cone-of-no-finite-elongation (Fig. 14-29d). After large strain, all material lines, initially tilted with respect to the plane of maximum constriction, will have rotated to near coincidence with the S_1-axis. Finite deformation patterns of competent single layers will then largely be limited to the cases illustrated in Figure 14-24c.

Figure 14-30 summarizes the progressive deformation of competent single layers in *coaxial oblate strain*. Layers coinciding with the S_1-S_2-plane of maximum extension will not rotate during progressive shortening but develop a pattern of chocolate-tablet boudinage. All other layers, initially inclined to the plane of maximum extension, will progressively rotate towards the S_1-S_2 plane of extension (stages 0 to 4). The fold axes perpendicular to the S_3-axis will unfold and material lines perpendicular to the fold axis will have resumed their initially straight orientation (*stage 3*) when rotated into parallelism with any of the lines making up the cone-of-no-finite-elongation. After large strain, all material lines, initially tilted with respect to the plane of maximum extension, will have rotated to near coincidence with the S_1-S_2-plane. Finite deformation patterns of competent single layers will then largely be limited to the cases illustrated in Figure 14-24d.

Coaxial plane strain, if studying the progressive deformation of material planes, is more complex than coaxial prolate or oblate deformations. This is because coaxial plane strain lacks the radial symmetry of oblate and prolate deformations. Instead, coaxial plane strain (pure shear deformation) is symmetric about the strain ellipsoid's S_1-S_2-plane (Fig. 14-31d). Figures 14-31a to d summarize the progressive deformation of competent single layers in *coaxial plane deformation*. The direction of maximum extension is parallel to the S_1-S_2-plane of the strain ellipsoid. Any layer initially tilted with respect to either the S_2- or S_3-axis, undergoes progressive deformation

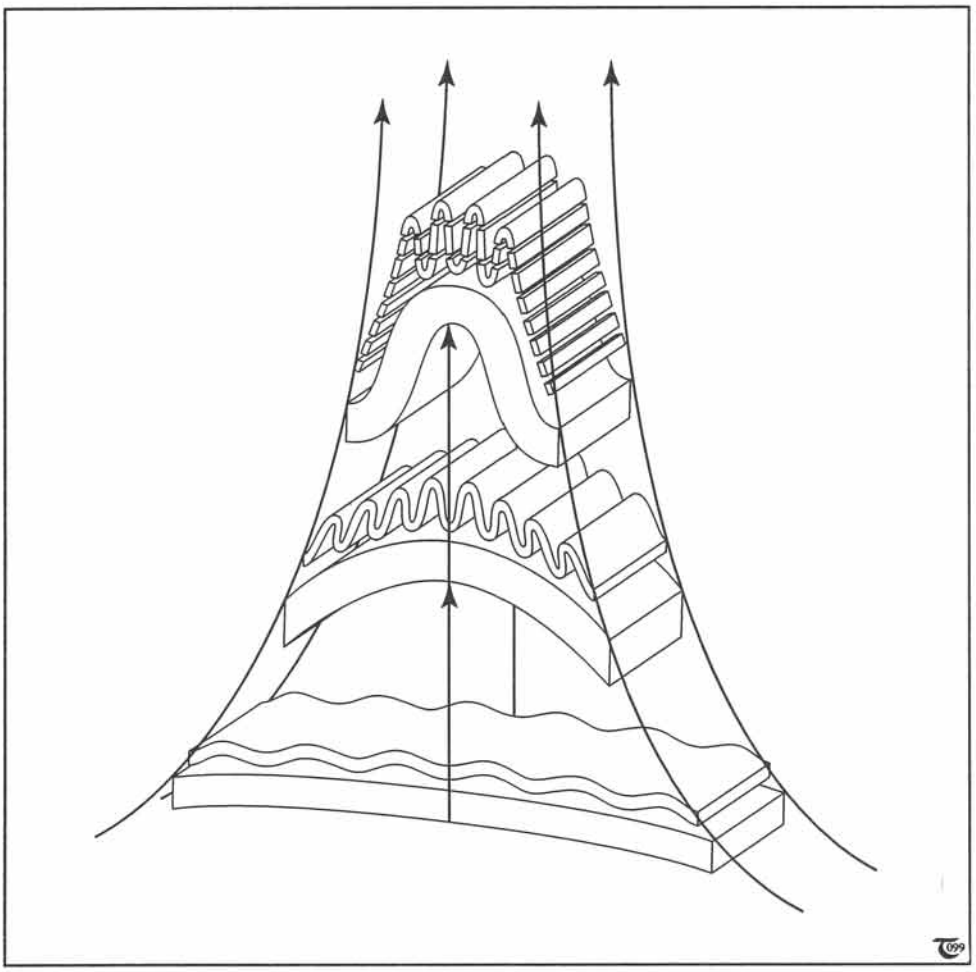

Figure 14-32: *Formation of asymmetric minor folds on the limbs of major fold closures. The buckling of a thick competent layer adjacent to a thin competent layer will tilt the limbs with respect to the bulk shortening axis. The wave length of folds in thicker layers is larger than that of folds in thinner layers, provided all other physical parameters (e.g. viscosity) are similar. The extensional flow axis coincides with the axial planes of major folds and remains perpendicular to the shortening direction if the bulk deformation is coaxial. The smaller wave length folds in the thinner layers and the progressive rotation of their limbs generate asymmetric minor folds with a consistent sense of asymmetry with respect to the major fold closure. The limbs of the minor folds may boudinage if rotated into the field of extension.*

involving rotation of the layer. This may lead to unfolding (Fig 14-31b) or fold axes, which reorient into parallelism with the extension direction (Fig. 14-31c).

Figure 14-31a illustrates how we generally perceive plane deformation of a competent single layer. The fold axes of a layer initially in the S_2-S_3 plane remain parallel to the S_2-axis at all times. The enveloping surface of the minor folds will not rotate, but their limbs may stretch into boudins if steeper than the planes-of-no-finite-elongation. Figure 14-31b shows how a competent single layer, comprising the S_2-axis but initially inclined to the S_3-axis, will first fold but then unfold, while rotating towards parallelism with the direction of maximum extension (S_1-axis). Material lines will have resumed their intially straight orientation (between stages 2 and 3) when rotated into parallelism with any of the lines making up the plane-of-no-finite-elongation. Figure 14-31c illustrates how a competent single layer comprising the S_3-axis, but initially inclined to the S_2-axis, will first fold but then unfold, while rotating towards parallelism with the direction of maximum extension. After large strain, all material lines, initially tilted with respect to the plane of maximum constriction, will have rotated to near coincidence with the direction of maximum extension. Finite deformation patterns of competent single layers will then largely be limited to the cases illustrated in Figure 14-24b.

Figure 14-32 illustrates the progressive deformation of two competent single layers into buckle folds. The rotation of the limbs of the minor folds in the thinner layer is faster than that of the limbs of the major folds in the thicker layer. Consequently, the minor folds are more likely to develop boudins, as compared to the major fold.

☐Exercise 14-20: The examples of progressive rotation and stretch of planes and the associated structures were confined to coaxial 3D deformation. a) Discuss why similar structures must form in non-coaxial 3D deformations. b) Explain why understanding non-coaxial 3D deformation is more difficult than understanding coaxial deformations.

References

A. Books

Folding and Fracturing of Rocks (1967, McGraw-Hill, 568 pages), by J.G. Ramsay. A classical text for structural geologists, interested in the detailed study of deformation patterns in rocks.

The Techniques of Modern Structural Geology. Volume 1: Strain Analysis (1983, Academic Press), by J.G. Ramsay and M.I. Huber. Beautifully illustrated and clearly writtten account on strain analysis with many detailed theoretical and practical exercises.

The Techniques of Modern Structural Geology. Volume 2: Folds and Fractures (1987, Academic Press), by J.G. Ramsay and M.I. Huber. Lavishly illustrated with photographs of folds, boudins, mullions and other rock structures encountered in the field.

B. Articles

Cloos, H. (1947, *Transactions of the American Geophysical Union*, volume 28, pages 626 to 632). Boudinage.

Flinn, D. (1962, *Quarterly Journal of the Geological Society of London*, volume 118, pages 385 to 433). On folding during three dimensional progressive deformation.

Ghosh, S.K. (1966, *Tectonophysics*, volume 3, pages 169 to 185). Experimental test of buckling folds in relation to strain ellipsoid in simple shear deformation.

Lloyd, G.E. and Ferguson, C.C. (1981, *Journal of Structural Geology*, volume 3, pages 117 to 128). Boudinage structures: some new interpretations, based on elastic-plastic finite element simulations.

Neurath, C. and Smith, R.B. (1982, *Journal of Structural Geology*, volume 4, pages 215 to 229). The effect of material properties on growth rates of folding and boudinage; experiments with wax models.

Paterson, M.S. and Weiss, L.E. (1968, *Geological Society of America Bulletin*, volume 79, pages 795 to 812). Folding and boudinage of quartz-rich layers in experimentally deformed phyllite.

Ramberg, H. (1955, *Journal of Geology*, volume 63, pages 512 to 526). Natural and experimental boudinage and pinch-and-swell structures.

Ramberg, H. (1959, *Norges geologiska Tidskrift,* volume 39, pages 99 to 152). Evolution of ptygmatic folding.

Selkman, S. (1978, *Tectonophysics*, volume 44, pages 115 to 139). Stress and displacement analysis of boudinage by the finite-element method.

Shimamoto, T. and Hara, I. (1976, *Tectonophysics*, volume 30, pages 1 to 34). Geometry and strain distribution of single-layer folds.

Smith, R.B. (1975, *Geological Society of America Bulletin*, volume 86, pages 1,601 to 1,609). Unified theory of the onset of folding and mullion structure.

Smith, R.B. (1977, *Geological Society of America Bulletin*, volume 88, pages 312 to 320). Formation of folds, boudinage, and mullions in non-Newtonian materials.

Smith, R.B. (1979, *American Journal of Science*, volume 279, pages 272 to 287). The folding of a strongly non-Newtonian layer.

Sokoutis, D. (1987, *Journal of Structural Geology*, volume 9, pages 233 to 242). Finite strain effects in experimental mullions.

Sokoutis, D. (1990, *Journal of Structural Geology*, volume 12, pages 365 to 373). Experimental mullions at single and double interfaces.

Strömgard, K.-E. (1973, *Tectonophysics*, volume 16, pages 215 to 248). Stress distribution during formation of boudinage and pressure shadows.

Weijermars, R. (1993, *Journal of Structural Geology*, volume 15, pages 911 to 922). Progressive deformation of single layers under constantly oriented boundary stresses.